arXiv:0706.4252v2 [nucl-th] 12 Jul 2007

Johann Wolfgang Goethe-Universität
Frankfurt am Main
Fachbereich 13, Institut für Theoretische Physik

&

Universitetet i Bergen
Institutt for fysikk og teknologi

# Mach cones in heavy ion collisions

Bjørn Bäuchle

June 2007

Diploma thesis

Advisor: **Horst Stöcker** & **László Pál Csernai**

*Für Hannah*

# Contents


**1 Introduction** **1**
1.1 What are we made of? . . . . . 1
1.2 Studying Quark Matter . . . . . 3
1.3 Supersonic acoustic sources . . . . . 5

**2 Models for heavy ion collisions** **9**
2.1 Thermal model . . . . . 9
2.2 Transport model . . . . . 10
2.3 Lattice QCD . . . . . 10
2.4 Hydrodynamical model . . . . . 10

**3 Jets and Medium** **15**
3.1 Calculated correlations in static medium . . . . . 19

**4 MACE — Mach Cones Evolution** **23**
4.1 Initialization and propagation of the jet . . . . . 24
4.2 The waves . . . . . 25
4.3 Freeze-out of the sound wave . . . . . 26
4.3.1 Trivial addition . . . . . 26
4.3.2 A coalescence-like model . . . . . 28
4.3.3 The Mantle Method . . . . . 29
4.4 Energy-conservation . . . . . 33
4.5 Perfect Background Subtraction . . . . . 34

**5 Results from MACE** **35**
5.1 Characterizing the algorithm . . . . . 36
5.2 Mach cones at RHIC . . . . . 38
5.2.1 Central collisions . . . . . 38

5.2.2 Mid-central collisions . . . . . 38
5.3 Mach cones at LHC . . . . . 41

**6 Summary and Outlook 47**

**A Bibliography 51**

**B Acknowledgements 57**

**C Legal stuff 59**
C.1 Zusammenfassung (German abstract) . . . . . 59
C.2 Erklärung zur Diplomarbeit (Declaration) . . . . . 63

# List of Figures


1.1 Phase diagram of QCD . . . . . 4
1.2 Sketch on mach cones . . . . . 6

3.1 Di-Jet-Suppression at $\sqrt{s_{NN}} = 200$ GeV . . . . . 16
3.2 Sideward peaks in two-particle correlations . . . . . 17
3.3 Scheme on three-particle correlations . . . . . 18
3.4 Three-particle correlations from STAR . . . . . 19
3.5 Calculated two-particle correlations in static medium . . . . . 22

4.1 Bullet in water . . . . . 27
4.2 Construction of the wave-lines . . . . . 32
4.3 Particle flow on the wave-lines . . . . . 33

5.1 Characterization of the code: different $m$ . . . . . 36
5.2 Characterization of the code: different $l$ . . . . . 37
5.3 Characterization of the code: different $d$ . . . . . 37
5.4 Central RHIC 2- and 3-particle correlations . . . . . 39
5.5 Mid-central RHIC 2- and 3-particle correlations . . . . . 40
5.6 Correlations: central LHC; arbitrary orientations, 3D . . . . . 41
5.7 Correlations: central LHC; arbitrary orientations, 3D . . . . . 42
5.8 Correlations: Rapidity trigger . . . . . 43
5.9 Correlations: Different origins of the Jet . . . . . 44

# Chapter 1

# Introduction

## 1.1 What are we made of?

Where we come from, where we are going to and what we are made of are questions that have been asked by humans at all times. In former days, the only answers that could be given were speculations by philosophers or claims by priests. Even nowadays, we cannot answer any of these three questions in a satisfiable way. But we have shifted the emphasis of them a little.

The quest for our origin is nowadays shifted to evolution and its means, and / or finally to the big bang that astrophysicists believe has happened about 13.7 billion years ago. No-one can answer the question where that big bang came from.

Defining our destiny is something that implies the need for forecasts; as our understanding for the other two questions grows, we gain more and more knowledge on how to forecast things. Still, a precise forecast on the world's state tomorrow will never be possible.

The third question remains: What are we made of? We can neither give a final answer here. But we have come an enormously long way from the believes of the old greeks, that everything consists of water (Thales) or maybe of the four elements fire, air, water and earth. In the 19th century, chemists found parts of the matter they considered indivisible, and they classified about 50 so called *chemical elements* that are built up from those indivisibles — the *atoms*. Nowadays we know 91 natural chemical elements and have synthesized several more; their number is about 114. We also found out that there exist differences between the atoms of a single element; their

masses vary. Atoms of different mass belonging to the same chemical element are called *isotopes*. We know about 2.500 different isotopes.

The sheer variety of classes of atoms (and the fact that we can synthesize more) indicates that these are not as indivisible as chemists thought in the first place. Indeed, already in 1909 Lord Earnest Rutherford of Nelson found that atoms — he experimented with gold — consist of a very heavy, positively charged core, called the *nucleus*, and a very light shell, which is negatively charged. It was soon identified that the shell consisted of the same particles that make up for electricity, the *electrons*. The nuclei, on the other hand, have been found to consist of *protons* and *neutrons*, the so-called *nucleons*. Roughly spoken, the number of protons in a nucleus determines the chemical element, whereas the number of neutrons distinguishes different isotopes. By those discoveries the variety of 2.500 different indivisible particles has been reduced to 3[1].

When trying to study electrons, protons and neutrons, further particles have been discovered. Besides particles that resemble light — the so-called *photons* — and similar particles, the new particles can be put into two classes: Those that interact with nuclear matter as nuclear matter itself does, i.e. with the so-called *strong force*, and those that don't. The first are called *hadrons*, the latter are *leptons*[2]. In the *standard model of particle physics*, which is the state-of-the-art-theory of our knowledge about matter, the six known types of leptons (called *electron*, *muon*, *tauon*, *electron-neutrino*, *muon-neutrino* and *tau-neutrino*) remain fundamental parts of matter. No experimental results indicate that they have an inner structure.

This is not the case for the hadrons. Hundreds of hadrons have been directly or indirectly detected, and it turned out that they are not fundamental. Instead, new degrees of freedom have been postulated and experimentally observed, so-called *quarks* and *gluons*. In accordance to the number of leptons, we know six quarks, called *up*, *down*, *charm*, *strange*, *top* and *bottom*, from which only up and down form neutrons and protons. Gluons are to the strong interaction what photons are to electrodynamics, the theory that covers electricity, magnetism and light.

Quarks and gluons are, as leptons and photons, considered fundamental parts of matter. Their observation, though, is not very easy. Due to

[1] For completion, it should be said that the electrons make up for the chemical properties of an element, but *their* number is determined by the number of protons in the nucleus.

[2] The terms have greek origin and mean "strong particles" (hadrons) and "light particles" (leptons), referring to the strong force and low masses, respectively.

the structure of the strong force and the underlying theory, the *Quantum Chromo Dynamics* (QCD), they can never be seen alone, but only in pairs (one quark and an antiquark) or in triplets (three quarks or three antiquarks), or any combination thereof. This phenomenon is called *confinement*. When scatterings between quarks happen at very high center of mass-energies, this confinement ceases to exist. This is called *asymptotic freedom*. It is subject to experimental research to create *deconfined* matter, i.e. matter that is asymptotically free. Since this matter consists of free quarks and gluons, it is called *Quark Gluon Plasma* (QGP).

## 1.2 Studying Quark Matter

The purpose of the largest experiments on earth, such as the Relativistic Heavy Ion Collider (RHIC) at Brookhaven National Laboratory (BNL), the Tevatron at Fermilab and — soon — the Large Hadron Collider (LHC) of the European Council for Nuclear Research (CERN), is to probe the smallest parts of matter we know. At these facilities, protons (Tevatron and LHC), gold- (RHIC) and lead nuclei (LHC) are accelerated to velocities very close to the speed of light and collided with each other. In proton-proton-collisions as the smallest possible system of colliding stable hadrons, the fundamental forces and particles can be studied in a very clean way, whereas in the bigger systems (gold on gold and lead on lead) collective properties of the matter can be studied.

The latter is the kind of physics that is addressed in this thesis. In systems with 396 or 416 initial nucleons (gold and lead, respectively), it can e.g. be studied how the single particles react in connection with and surrounded by many other particles. Quantum Chromo Dynamics (QCD), the gauge theory for strong interactions, predicts free quarks and gluons in the infinite high temperature limit. It is hoped that this "deconfinement" can be reached in collider experiments. Indeed it is claimed to have been seen in experiments at the Super Proton Synchrotron (SPS) at CERN [1] and at RHIC.

When studying heavy ion reactions, a major field of interest is the so-called *phase diagram* of QCD. Like in everyday physics, such a diagram shows in what state the matter is at given conditions. Unlike in everyday physics, the conditions are not given in pressure and temperature, but in (baryo-)chemical potential $\mu_B$ and temperature $T$ (see figure 1.1). Depending on the *center of mass-energy* $\sqrt{s_{NN}}$ of the collision and on the system size

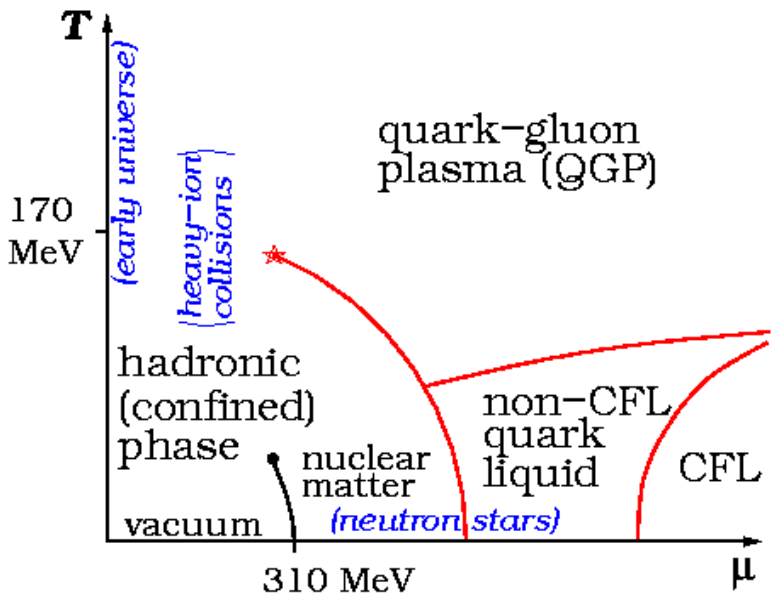


Figure 1.1: The phase diagram of QCD. It shows the different expected phases. At $\mu = 310$ MeV and $T = 0$ lies ground state matter. Note that the position of phase transitions is not known exactly. From [3]

(determined by the nuclei involved) one can probe different regimes of the diagram. With very high energies and big nuclei the matter is heated very much (high $T$), but has few baryons (low $\mu_B$). Such matter is created at RHIC and LHC. Here, a second order phase transition is believed to occur at a temperature $T_C \approx 170$ MeV [2].

This phase-transition leads from a gas of normal, confined hadrons, the *Hadron Gas* (HG), to deconfined Quarks and Gluons, the *Quark-Gluon-Plasma* (QGP). This phase seems to behave like a liquid, according to claims made by the experiments at RHIC [4]. This is surprising, because it has previously been thought of as a perfect gas.

The theoretical problem one has when dealing with nuclear matter is that QCD cannot be solved perturbatively at small energy-momentum transfers $Q^2$. This is due to the at low $Q^2$ large coupling constant. Unlike the electromagnetic coupling the strong coupling varies a lot and actually falls with increasing $Q^2$, which is the reason for the theory being "asymptotically free". For lower temperatures (and therefore lower $Q^2$), nuclear systems cannot be

calculated from first principles (namely QCD), but with effective models. Some of these are described briefly in chapter 2. Also, the concept of temperature itself introduces the need for many particles, and there is no kind of interaction in which many-particle systems can be described exactly. This is another reason for the need of effective models, even above the threshold for deconfinement.

Of the existing models for dynamical descriptions of heavy-ion reactions (see chapter 2), hydrodynamics is very popular. In this approach, the matter is described as a fluid. Hence, collective effects can be studied easily. For example, collective flow is an observable intimately connected to hydrodynamic behaviour (for more detail, see section 2.4).

## 1.3 Supersonic acoustic sources

In all fluids, there exists a mode for propagating weak, linear perturbations. Those perturbations are exactly what excites the human eardrums and causes us to hear — *sound*. The speed with which these perturbations move is the largest speed by that any mechanical stimulus can travel through a given body (which does not necessarily have to be a liquid) and depends on the material the body consists of. It might also depend on the wavelength of the perturbation, this phenomenon is known as dissipation and does not exist in perfect liquids.

The speed of sound $c_S$ can be calculated from the Equation of State (EoS, see section 2.4, page 12) to be the partial derivative of the pressure $p$ with respect to the energy density $e$

$$c_S^2 = \frac{\partial p}{\partial e} \quad . \tag{1.1}$$

When an acoustic source moves through a medium, the audible sound changes. A resting observer in front of the source will hear a higher frequency than is actually emitted, if the source passed her, she will hear a lower frequency. This phenomenon is known as the *Doppler-effect*. It can be easily understood if one considers the sound waves emitted by the source as being compressed in forward direction and elongated in backward direction.

If the speed of the source is the same as the sound velocity, all sound waves ever emitted by it will reach the observer at the same instant — together with the source itself. One cannot hear no frequency anymore, but only a

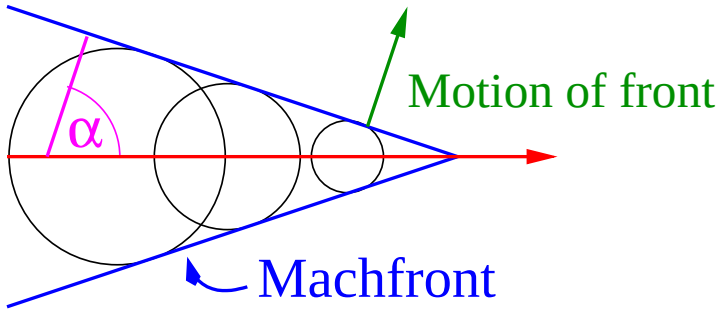


Figure 1.2: A schematic view on how a mach cone develops (in two dimensions): The elementary sound waves all add up at one line. The angle $\alpha$ is given by $\cos(\alpha) = c_S/v$, where $v > c_S$ is the velocity of the source.

*(super)sonic boom.* In the supersonic regime, when the source is moving faster than the sound it emits, the sound arrives after the source has passed. The waves form a cone — the *mach cone*, named after Ernst Mach, an Austrian physicist who lived from 1838 until 1916. The cone develops because there is a straight surface perpendicular to every elementary sound wave emitted at any instant, see figure 1.2.

Unlike normal sound perturbations, the amplitude of the mach cone does not decrease with the square of the distance to the exciter, since it is not a point, but only with the distance to the first power, since the exciter forms a straight line (this is analogous to the electrical field of a pointlike charge and a infinitely long, homogeneously charged wire).

Measuring the angle of a mach cone will give insight on the speed of sound or the speed of the particle, if the respectively other is known. Therefore it might help to falsify an assumed Equation of State for the medium considered.

Whereas in everyday experience, the velocity of the medium, say, air, is small in comparison to the speed of sound and its fluctuations therefore are small as well, this is not the case in general. In nuclear matter, collective motion may be as fast as and even faster than the speed of sound and vary a lot along the trajectory of the sound source. To study how much this affects the resulting shape of a mach cone is the goal of this thesis.

In our special case, we consider a high energy jet, as might result in a partonic collision in the very early stages of a heavy ion reaction, and

examine the sound waves it emits and their way through a realistic medium that moves with a speed comparable to the speed of sound itself (something that will never be seen in everyday physics).

# Chapter 2

# Models for heavy ion collisions

## 2.1 Thermal model

Since the transverse momentum spectra of particles in heavy ion collisions are pretty similar to what is predicted by thermodynamical assumptions, they are sometimes described as coming from a source that is globally equilibrated [5, 6, 7, 8, 9, 10].

The model starts with the phase space density, which is given as

$$f(x,p) = \frac{\mathrm{d}N}{\mathrm{d}\Gamma} = \frac{\mathrm{d}N}{\mathrm{d}^3x\,\mathrm{d}^3p} = \frac{g}{(2\pi)^3}\frac{1}{\exp\left(\frac{E-\mu}{T}\right)+\alpha} \quad . \tag{2.1}$$

Here, $E = \sqrt{\vec{p}^2 + m^2}$ is the energy, which will in the more general case of a moving source (moving with the four-velocity $u^\mu$) be replaced by the scalar product $p_\mu u^\mu$. $g$ and $\mu$ denote the degeneracy factor and chemical potential for the particle species considered, and $T$ is the temperature. The latter is assumed to be the same for all species. $\alpha$, finally, distinguishes the different spin statistics: For bosons (integral spins), it is $\alpha_{\mathrm{BE}} = -1$, which results in the Bose-Einstein-distribution, whereas for fermions (half-integer spin) it is $\alpha_{\mathrm{FD}} = +1$, which leads to the Fermi-Dirac-distribution. For high energies and high temperatures both distributions become equal, $\alpha$ can be neglected, and one obtains the Maxwell-Boltzmann-distribution.

A thermal model is by far the most macroscopic approach to heavy ion collisions. It can not account for local inhomogeneity and its applicability to a system exploding immediately and with high velocities is highly questionable.

## 2.2 Transport model

An approach that accounts not only for local deviations from an assumed global symmetry, but really tries to model each particle and its trajectory through the space time, is the transport approach [11, 12, 13]. The evolution of the system follows the relativistic transport (or *Boltzmann*-) equation

$$p^\mu \partial_\mu f(x, p) = \mathrm{St}\{f\} \tag{2.2}$$

Here, $\mathrm{St}\{f\}$ is called the collision term, which contains information on cross-sections and acts as source term for the density function.

A set of solutions to that formula is the equilibrium phase space density used for thermal and hydrodynamical models (2.1).

Transport models assume point like, classical particles whose mean free path is very large. The description of three-particle-collisions is very complicated.

## 2.3 Lattice QCD

An approach to solve the equations of QCD directly is to perform lattice calculations. Here, space and time are descretised (therefore "lattice"). The properties of infinitely vast matter in equilibrium, and therefore the Equation of State, can be studied [14, 15, 16, 17, 18]. It does not provide a dynamical description, but can give exact input to hydro- and thermodynamical models.

## 2.4 Hydrodynamical model

A model widely used to describe heavy-ion reactions is fluid- or hydrodynamics. It has been predicted as a key mechanism for the creation of hot and dense matter very early [19, 20]. Using this approach one assumes that the matter described is in local thermal equilibrium or at least in a state showing only small deviations from that. This assumption is not obviously met in a heavy ion reaction. Indeed, seen from any frame, the particle distribution functions of projectile and target are very different and far from being equilibrated. In the progress of the collision, though, a locally equilibrated system may be formed. The part of the reaction before equilibration can therefore not be described by usual (1-fluid-) hydrodynamics.

One approach is to introduce several distinct fluids that each hold a equilibrated subsystem, e.g. one fluid for the target, one for the projectile and optionally a third for the evolving fireball. The whole system here is not equilibrated, but hydrodynamical evolution of each component is possible. Interaction between the components is implemented by considering the other components as source terms in the equations.

This approach allows for modelling of transparent nuclei, i.e. of the fact that at low energies the nuclei penetrate through each other.

In so-called *one-fluid hydrodynamics* the beginning of the reaction cannot be modelled. Therefore, an additional model has to be applied for the creation of the first equilibrated state, the so-called *initial state*. This can in principle be any kind of non-equilibrium model. The creation of the first equilibrated state can take different times, depending on the mechanism with which it is reached. Times of the order of $\tau_0 \approx 1$ fm are reasonable.

When the initial state is defined, hydrodynamics start to work. Depending on number and kind of the assumed symmetries in the initial state the fluid development may be solvable analytically or only numerically. Within this stage of the calculations, one has to assume an equation of state (EoS). It must also be chosen if the evolution describes a perfect fluid that is perfectly equilibrated at any point or if small deviations are endorsed. In the latter case, several additional parameters like the heat conductivity, shear- and bulk-viscosity have to be introduced.

In the case of a heavy ion collision the reaction zone is surrounded by vacuum, into which the matter will expand. Therefore, the energy-density and the particle density will decrease as a function of time. The system gets more and more dilute, and the assumption of local equilibrium at any point gets more and more unjustified. A condition has to be defined where the hydrodynamical evolution is stopped and something else is done. This step is called *freeze-out*. Whatever the condition is — specific lab- or proper-time, temperature, energy density, baryon number density —, it must be such that each part of the system crosses that condition and can be frozen out. The area in which freeze-out happens is usually a three dimensional *hyper-surface*, but it might have a finite thickness, which would lead to a hyper-layer or hyper-volume.

Apart from the choice of the position of the surface, some other things may be adjusted for the freeze-out process. This starts with the kind of matter in the final state. Here, massive hadrons, massive quarks (without hadronisation so far), even massless quarks or hadrons may be assumed.

Quantum effects in the distribution function may or may not be taken into account.

In any case, freeze out should conserve some quantities. Besides energy-momentum- and baryon number-conservation care has to be taken that entropy does not decrease. It is an additional constraint to require even the gross baryon number (number of baryons plus number of antibaryons) to be equal across the freeze-out process.

Even for the surface it is not enough to state its position, its thickness has to be taken care of as well. While the classical, standard approach considers it to be infinitely small, it may also be that freeze-out happens at a whole layer, which implies that particles may leave the system that are close to, but not at the bordering condition.

Starting with the Boltzmann transport equation (2.2) with a vanishing source term, one can define *moments* of the distribution as

$$N^\mu(x) = \int \frac{\mathrm{d}^3 p}{p^0} p^\mu f(x,p) \tag{2.3}$$

$$T^{\mu\nu}(x) = \int \frac{\mathrm{d}^3 p}{p^0} p^\mu p^\nu f(x,p) \tag{2.4}$$

which are the baryon number current and the energy-momentum density, respectively. Since $p^\mu \partial_\mu f = 0$ (see (2.2)), it follows that

$$\partial_\mu N^\mu = 0 \tag{2.5}$$

$$\partial_\mu T^{\mu\nu} = 0 \quad . \tag{2.6}$$

These five equations (there is one for every $\nu$ in (2.6)) face fourteen independent variables whose time developments have to be found (four independent components of $N^\mu$ and 10 independent components of the symmetric four by four-tensor $T^{\mu\nu}$). By assuming perfect local thermal equilibrium 8 independent components of $T^{\mu\nu}$ can be eliminated. Then, one is left with 6 parameters and only needs one more equation — the equation of state (EoS). This usually gives a relation between pressure, energy density and baryon number density. For a detailed description on how to decompose $T^{\mu\nu}$ into a ideal and non-ideal part and the different possibilities for various definitions please refer to [21, 22].

Very simple equations of state consider ideal, ultra-relativistic (i.e. massless) gases. Here, the speed of sound is constant $c_S^2 = 1/3$. The pressure is

not dependent on the baryo-chemical potential. This EoS is considered good in the QGP-regime. For lower temperatures, the simplest case is a (massive) hadron-resonance-gas. Here, the speed of sound is given by $c_S^2 = 0.15$.

**The hydrodynamical model** used in this thesis is the *particle in cell* (PIC)-method which has been developed by Harlow and Amsden in the early 1960s [23, 24] and upgraded to ultra-relativistic energies by Nix and Strottman in the 80s and 90s [25, 26, 27]. It combines the advantages of fixed cells (Eulerian grid) and free moving particles (Lagrangian markers) and has e.g. explicit baryon number conservation. An ideal gas with two flavours is assumed for the Equation of State. It has a constant speed of sound $c_S = 1/\sqrt{3}$. The initial state has been developed recently by Magas, Csernai and Strottman and is exhaustively explained in [28]. Freeze-out happens at constant time and goes from massless QGP to massive quarks with a restmass of $m_q \approx 300$ MeV. Hadronisation is abjured [29]. It conserves energy, baryon number and gross baryon number.

# Chapter 3

# Jets and Medium

In any collisions of the kind $2 \rightarrow 2$ (i.e. two incoming particles produce two outgoing particles), the daughter particles will be, seen from the center of mass system, back-to-back-correlated. This is a simple consequence of conservation of momentum. When the momentum transfer $Q^2$ in a collision becomes sufficiently large, the structures that play a role for scatterings become small enough not to resolve whole hadrons, but their constituents, the partons. In other words, at high energies partonic interactions dominate over hadronic interactions. In this region also *perturbative QCD* (pQCD) is applicable, because the strong coupling constant $\alpha_S$ is small enough.

When two partons scatter, their daughter particles usually fragment into hadrons after a short time, that means they create new $q\bar{q}$-pairs from the vacuum, thereby losing energy and form hadrons themselves as well as new hadrons, that typically go parallel to the leading hadrons. Theses bunches of hadrons are called jets.

If nothing hinders the jets from being detected, as is the case in proton-proton collisions, two jets will be seen that are usually exactly back-to-back-correlated. The center of mass of very high energetic partonic collisions is usually the same as the center of mass of the proton-proton collision.

When correlating the azimuthal angles $\varphi$ of the observed hadrons one can recognize such events by two peaks at $\Delta\varphi = 0$ and $\Delta\varphi = \pi$. This signal for *di-jets* is seen in *pp*-collisions at high energies.

In heavy ion collisions, it is not so clear whether such a signal can be seen. The created jets might have to penetrate through the medium that is present in such reactions, except when the initial parton-parton collision happens at the surface of the medium and both daughter particles go tangential to the

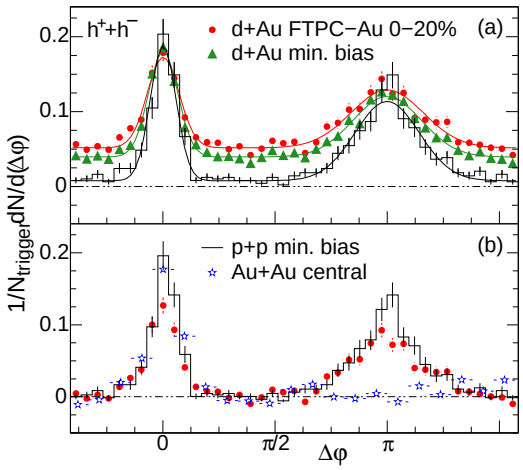


Figure 3.1: Two particle correlations for p+p, d+Au and Au+Au-collisions at $\sqrt{s_{NN}} = 200$ GeV. Trigger particles are in $4\,\mathrm{GeV} < p_{\perp\mathrm{Trig}} < 6\,\mathrm{GeV}$, and associated particles are all those with a momentum bigger than 2 GeV and less than the trigger $2\,\mathrm{GeV} < p_{\perp\mathrm{assoc.}} < p_{\perp\mathrm{Trig}}$. The curves show a clear suppression of secondary particles at $\Delta\varphi = \pi$ in gold-gold-collisions when compared to the smaller systems. From [30].

surface. In all other cases, at least one of the jets has to go through the medium. Indeed, the most interesting case is a hard collision close to the surface with one daughter going right out of the collision zone and the other going the longest possible way through it. Here, studying the so-called *near-side-jet* (the one leaving the system immediately) can give insight on the parameters of the original hard collision and on the parameters of the *away-side-jet*.

Depending on the properties of the medium the away-side-jet will look different to the experiment. For example, the cross-section for interactions between jet and medium might be very small, or the medium dilute enough, so that the jet goes through the medium almost undisturbed. This is the case at (comparatively) low energies.

At central RHIC collisions, however, there is no away-side-jet observed with an energy comparable to the near-side-jet [30], see figure 3.1.

Obviously, the away-side-jet loses its energy, which is in return absorbed in some way by the medium. Different models for this energy loss exist,

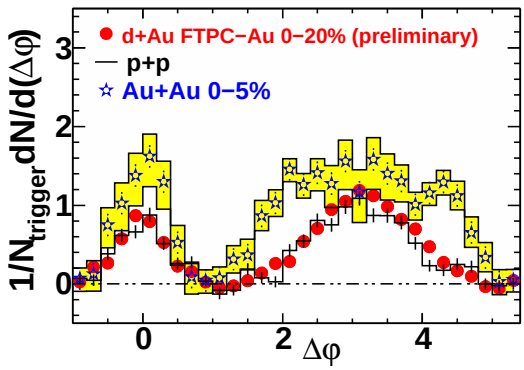


Figure 3.2: Two particle correlations for p+p, d+Au and Au+Au-collisions at $\sqrt{s_{NN}} = 200$ GeV with same threshold for trigger particles as in figure 3.1, but lower trigger for associated particles $0.15\,\mathrm{GeV} < p_{\perp\,\mathrm{assoc.}} < 4\,\mathrm{GeV}$. The data show sideward peaks at $\Delta\varphi \approx \pi \pm 1$. From [47].

and the exact mechanisms are subject to current discussion in the field. A long time [31, 32, 33, 34, 35] radiative energy loss has been considered the dominant mechanism. In 2003, Mustafa and Thoma [36] re-considered energy loss by collisions, as had been predicted long before [37, 38, 39, 40]. Only recently, Mustafa and Thoma's results gained more attention [41]. Peshier [42, 43, 44, 45] has shown in 2006 that collisional energy loss is indeed very important for the explanation of the magnitude of transport coefficients etc.

In any case, secondary particles will have significantly lower momentum than the near-side-jet, which is a good explanation to the apparent complete disappearance of the away-side-jet in [30]. When lowering the threshold for secondary particles, one can see sideward peaks in the two-particle azimuthal correlations [46], see figure 3.2. Such a signal has been predicted as signature for mach shocks in 2004 [48]. But also large-angle gluon radiation [49, 50], jets deflected by radial flow and čerenkov radiation [51, 52] are consistent with the observed away-side structure.

Mach cones in nuclear matter have been predicted for cold nuclear matter [19, 53, 54, 55, 56], fermi liquids [57, 58] and QGP [59, 60, 61] and observed in heavy ion reactions at RHIC [62, 63, 64, 65, 66, 67, 68, 69, 70].

Recently, the predictions are supported by measured three-particle correlation spectra, where two azimuthal correlations are being opposed (see figure 3.3). Here, a clear distinction can be made between an indifferent en-

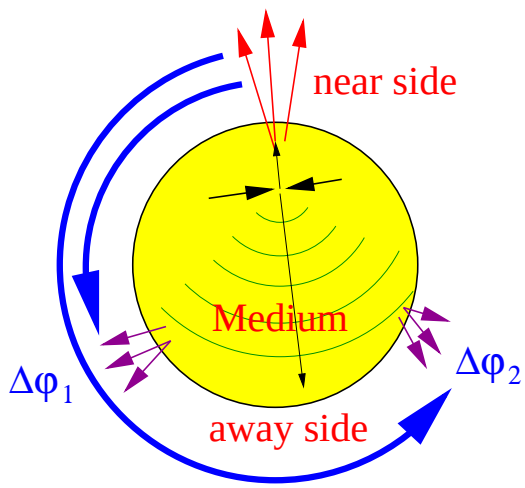


Figure 3.3: This sketch shows the angles used for three-particle correlations. Azimuthal differences from two different particles to the high-$p_\perp$-particle are opposed.

hancement of spectra by deflection etc. and mach cones or čerenkov radiation that pronounce explicit directions. Peaks at $(\Delta\phi_1, \Delta\phi_2) = (\pi \pm b, \pi \pm b)$ (on the bisector) would be present in all scenarios, they correspond to the fact that a jet typically consists of more than one particle, and a peak on the bisector merely says that two particles are emitted at the same angle. Peaks at $(\Delta\phi_1, \Delta\phi_2) = (\pi \pm b, \pi \mp b)$ (note the opposite sign!), on the other hand, show a correlation between markers on *both sides* of the backward direction.

To distinguish between čerenkov radiation and mach cones, one can look at the $p_\perp$-dependence of the angle. In [51] it is shown that the angle of the čerenkov cone should be increasing very quickly with the momentum of the associated particles.

Preliminary data from STAR (see figure 3.4) support the conical mechanisms (mach cones or čerenkov radiation), and deeper insight leave, according to [71], little doubt on the dominance of mach cones over čerenkov radiation.

Satarov [72] and Chaudhuri [73] have calculated that the jet angle in an expanding medium is also very dependent on the exact origin of the jet. In short, the angle rises when the jet does not come from the middle of the medium.

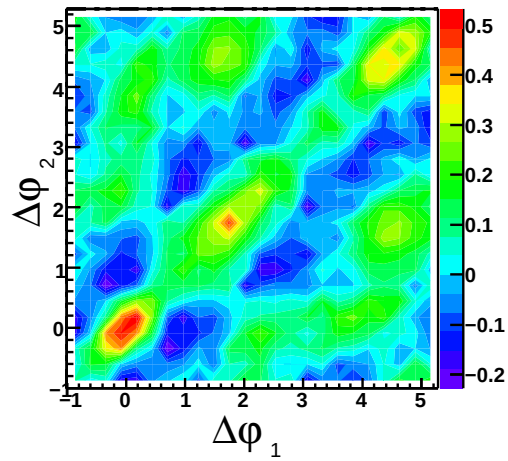


Figure 3.4: Three-particle correlations from STAR. $b$ (see text) is about 1.1 radians $\equiv 63°$ here, which corresponds (in static medium) to a speed of sound of $c_S^2 \approx 0.21 \pm 0.8$. See text for more details. From [71].

## 3.1 Calculated correlations in static medium

It is not trivial to calculate the expected angular distribution even for static medium. The reason for that is that one has to use two different coordinate systems, both of which are spherical. One is the laboratory system, having the beam axis as the pole, the other one having the jet axis as pole. Describing the cone is very easy in the latter, which will be denoted $(\alpha, \beta)$ for polar- and azimuthal angle, but the measured angle will be seen from the outside system $(\vartheta, \varphi)$. Both systems never are the same, because the jet can — in the model used — never go into the beam direction (see chapter 4).

A jet propagating through static medium will cause a cone appearing at a constant longitude, in the system where the jet is going towards the pole. The angular distribution is here

$$\frac{\mathrm{d}N}{\sin(\alpha)\,\mathrm{d}\alpha\,\mathrm{d}\beta} = \delta\left(\cos(\pi - \alpha) - c_\mathrm{S}\right) \quad , \tag{3.1}$$

or, in other words, the cone is at

$$\hat{r}_{\alpha\beta} = \begin{pmatrix} \sin(\pi - \alpha_0)\cos(\beta) \\ \sin(\pi - \alpha_0)\sin(\beta) \\ \cos(\pi - \alpha_0) \end{pmatrix} \quad , \tag{3.2}$$

where the index $\alpha\beta$ defines the coordinate system to have the $\hat{z}$-axis in the direction of the pole, which is the direction of the jet. Here, $\cos(\pi - \alpha_0) = -\cos(\alpha_0)$ is fixed to the speed of sound (it is the usual mach angle), but $\beta$ runs around the circle: $\beta \in [0; 2\pi)$. Each point on this circle is equally weighted with spectral enhancement, so that $\mathrm{d}N/\mathrm{d}\beta = const$. Note that, as long as one stays consistent within one consideration, the exact choice on the $\beta = 0$-direction is arbitrary, therefore, at the start, $\cos(\beta)$ and $\sin(\beta)$ are interchangeable. A relative negative sign will occur if a jet in positive and negative beam direction are considered, because the direction of rotation of $\beta$ has been changed.

In order to obtain the spectrum $\mathrm{d}N/\mathrm{d}\varphi$ as measured in a heavy ion experiment, one has to rotate the system $\alpha\beta$ to $\vartheta\varphi$. For a jet at mid-rapidity this is simple. In the following, the jet will always go in $\hat{x}$-direction, where the azimuthal angle is zero (this is equivalent to using the difference angle $\Delta\varphi$). Then, the cone will be at

$$\hat{r}_{\vartheta\varphi} = \begin{pmatrix} \cos(\alpha_0) \\ \sin(\alpha_0)\cos(\beta) \\ \sin(\alpha_0)\sin(\beta) \end{pmatrix} \quad . \tag{3.3}$$

Now, the azimuthal angle $\varphi$ can be read off:

$$\tan(\varphi) = \frac{y}{x} = \tan(\alpha_0)\cos(\beta) \quad . \tag{3.4}$$

$\mathrm{d}N/\mathrm{d}\varphi$ can be expressed as $\mathrm{d}N/\mathrm{d}\beta \cdot \mathrm{d}\beta/\mathrm{d}\varphi$, where the first factor is one (see above). The latter can be obtained from equation (3.4):

$$\beta = -\arcsin\left(\frac{\tan(\varphi)}{\tan(\alpha_0)}\right) \tag{3.5}$$

$$\frac{\mathrm{d}\beta}{\mathrm{d}\varphi} = \frac{-\left(1 + \tan^2(\varphi)\right)}{\sqrt{\tan^2(\alpha_0) - \tan^2(\varphi)}} \quad . \tag{3.6}$$

For the minus-sign in equation (3.6) refer to the statement above.

In the case of a jet that is not going to mid-rapidity, the formulæ become a lot more complicated. To characterize the direction of the jet, we take the angle $\tau$ between the direction of the jet and mid-rapidity. Thus, $\tau = \pi/2 - \vartheta$. The general idea is the same as before; we rotate $\hat{r}_{\alpha\beta}$ (see equation (3.2)) to $\hat{r}_{\vartheta\varphi}$, solve for $\beta$ and derive with respect to $\varphi$.

The rotation now happens with a more complicated matrix; we rotate around the $\hat{y}$-axis with an angle of $\tau$:

$$\hat{r}_{\vartheta\varphi} = \begin{pmatrix} \cos(\tau) & 0 & +\sin(\tau) \\ 0 & 1 & 0 \\ -\sin(\tau) & 0 & \cos(\tau) \end{pmatrix} \begin{pmatrix} \cos(\alpha_0) \\ \sin(\alpha_0)\cos(\beta) \\ \sin(\alpha_0)\sin(\beta) \end{pmatrix} \tag{3.7}$$

$$= \begin{pmatrix} \cos(\tau)\cos(\alpha_0) + \sin(\alpha_0)\cos(\beta)\sin(\tau) \\ \sin(\alpha_0)\sin(\beta) \\ \cos(\tau)\sin(\alpha_0)\cos(\beta) - \cos(\alpha_0)\sin(\tau) \end{pmatrix} . \tag{3.8}$$

As before, we read off $\tan(\varphi)$ as the ratio of y- and x-component. Using $A\cos(\phi) + B\sin(\phi) = \sqrt{A^2+B^2}\cos(\phi - \arctan(B/A))$ and basic geometry one finds

$$\beta = \arccos\left(\frac{-\cos(\tau)\tan(\varphi)}{\tan(\alpha_0)}\sqrt{\frac{1}{1+\sin^2(\tau)\tan^2(\varphi)}}\right) + \arctan\left(\frac{1}{\sin(\tau)\tan(\varphi)}\right) \tag{3.9}$$

and, after some more calculations,

$$\frac{\mathrm{d}\beta}{\mathrm{d}\varphi} = \frac{1+\tan^2(\varphi)}{1+\tan^2(\varphi)\sin^2(\tau)}\left\{-\sin(\tau) + \cos(\tau) * \right. \\ \left. * \sqrt{\frac{1}{\tan^2(\alpha_0)+\tan^2(\varphi)\left[\tan^2(\alpha_0)\sin^2(\tau)-\cos^2(\tau)\right]}}\right\} . \tag{3.10}$$

Although equation (3.10) seems very complicated, two special cases can be examined very easily. For $\tau = 0$, which corresponds to a jet in mid-rapidity, one can re-obtain equation (3.6), and for $\tau = \pm\pi/2$ one can as well easily see that the result is $\mp 1$, which is expected because in these cases (the jet goes along the $\hat{z}$-axis) $\varphi$ and $\mp\beta$ are equal. The function is plotted for three different $\tau$, namely 0, 30 and 60 degrees, in figure 3.5.

For certain angles $\tau$, the distribution (3.10) is obviously undefined. In the cases where the root gets imaginary, there are no particles emitted, the distribution should hence be set to zero. In the cases where the root diverges, a divergent measurement will be prevented by the fact that what is measured in an experiment is always the average of the distribution function over a small interval.

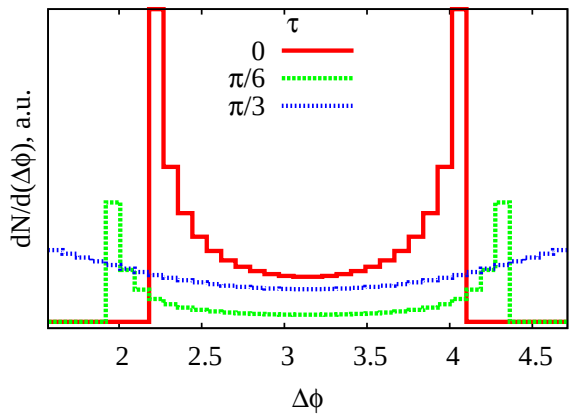


Figure 3.5: Calculated two-particle correlations in static medium. Shown are the correlations for a jet at mid-rapidity (solid line), for a jet at $\tau = 30°$ (dashed line — $\pi/6$) and at $\tau = 60°$ (dotted line — $\pi/3$) in the backward hemisphere. It can be seen how the maximum wanders "outside".

However, at the border of the defined interval there is a peak. With the modulus of $\tau$, $|\tau|$, getting bigger, the defined interval gets bigger. For mid-rapidity it is $\mathcal{D} = (\pi - \arccos(c_S), \pi + \arccos(c_S))$, but for all other jets it will be larger. No jet will therefore contribute a peak between the mid-rapidity-peaks, but only outside. Therefore, the maximum of the distribution function will shift "outwards", i.e. it will suggest a smaller speed of sound[1]. Note that this effect always draws in one direction, and only a measurement at absolute mid-rapidity may reveal the true speed of sound — but then again, this all is for a static medium only.

[1]Of course, this could be shown by integrating equation (3.10) over $\tau$ and analyzing the resulting function. We rather take the figurative approach.

# Chapter 4

# MACE — Mach Cones Evolution

In order to study mach cones in a medium with realistic behaviour, a model has to be built that either creates cones together with the medium (so that the cones become an inherent part of the evolution) or one that does add cones to the medium with hindsight, as perturbations.

The first case requires the evolution algorithm to have a much higher spatial resolution than it would be reasonable to have for a hydro-code, else small (and localized) perturbations would be lost very quickly. Propagating a jet as a very strong perturbation within a locally equilibrated medium is at least a questionable thing to do. The arising dilemma would be eliminated if one only propagated the sound waves within the equilibrated system and considered the jet being an external source of energy and momentum that, if it is affected by the medium at all, only interacts outside of the hydro framework.

In the latter case, on the other hand, backreaction towards the system has to be neglected. This is, though, a quite reasonable choice for sound-like perturbations which are expected to be small (else they are not sound-like any more). But regrettably also energy-conservation is not fulfilled. Neither the energy of the jet nor the additional momentum which in the end will be calculated can be taken out of the system but have to be added. Therefore, one has to assume that the total energy is much bigger than the energy added. This, too, is not very hard to argue for; even at RHIC energies ($\sqrt{s_{\mathrm{NN}}} = 200$ GeV) adding a single 50 GeV-Jet (which is tremendously high) would only change the total energy by 0.13 %.

Adding waves to the system after the evolution is calculated allows for a much higher resolution; the position of a wave can in principle be specified up to the precision of floating-point operations at the calculating machine, whereas in the other case one was limited to the grid size used for the system.

Our approach is to take an existing hydro-evolution and impose a jet and the waves it creates after that as perturbations.

## 4.1 Initialization and propagation of the jet

Only the away-side-jet is considered, since the near-side-jet is not affected by and does not affect the medium.

The jet starts from a random position within the medium at the first timestep calculated by the hydrodynamical code. This is, depending on the system considered, after few $fm$ after the first collisions.

The jet is created at a given point with a probability that is proportional to the energy-density at that point. The jet's direction is totally random. This is a reasonable thing to demand, since we consider an equilibrated system, in which collisions in any direction may occur. So, even with solid angle-dependent cross-sections one will get a spherical symmetric distribution of secondary particles[1]. The only cut that is reasonably made is that we exclude all jets that will not end up in the detector. More specifically, we exclude for these studies all jets with a pseudorapidity $|\eta| < 0.9$, which is the acceptance of the ALICE-TPC [74]. This corresponds to an opening angle of $\Delta\theta \approx 88.5°$ and to a covering of about 70 % of the solid angle.

The jet is considered to be high energetic enough not to change its velocity and direction. Calculation of jet quenching is not within the scope of this thesis. It hence propagates in a straight line with speed of light through the medium and excites sound waves as it goes along. Its (final) direction will be used for correlation considerations in the end. When out of the medium, the jet does not excite sound waves anymore.

[1]This does not apply to the final measured momentum distribution, but it must be true if we take each collision by itself.

## 4.2 The waves

No premature assumptions on the shape of a resulting mach front can be made in an unforeseeable, inhomogeneous and non-statical medium. The reshaping of a mach front after boosting in and out of the fluid rest frame (FRF) and considering various alignments between the jet's and the fluid's direction have been discussed in several publications [72, 75, 76, 73], but none of them took into account a spatially inhomogeneous [72, 75] or a realistic, three-dimensionally evolving [76, 73] system. Also, they considered only the wave front.

We take a different approach: we will propagate the single elementary waves and identify the wave fronts independent of the propagation. This allows for parts of the elementary waves to become a part of a wave front only after some time and possible deflection. Also, some parts may be swamped away out of the wave front.

So, in order to model the sound waves we create a lot of logical particles, so-called *wave markers*, at the position of the jet. The word "logical" refers to the fact that we do not assign any physical quantities to these markers yet; they only represent the position of the wave. The number of these wave markers per timestep is an adjustable (and numerical) parameter, in the standard setting it is $n_{\text{markers}} = 1\,000$. The entirety of the wave markers sent out at one timestep will be referred to as one *elementary wave*. The markers will be assigned random directions, so that after a short propagation in homogeneous medium one elementary wave should indeed be a spherical wave. Such an elementary wave is created at each timestep. Between the timesteps all "waves", i.e. all wave markers, are propagated.

The propagation of the wave markers is straightforward: The only assumption made is that they move with the speed of sound relative to the fluid wherever they are. Their direction is adjusted by relativistically adding their initial velocity, $\vec{v}$, to the flow-velocity of the underlying medium at the current point, $\vec{u}$. Technically, this is done by adding the vectors corresponding to the respective rapidities $\vec{y}_v$ and $\vec{y}_u$:

$$\vec{v}\prime = \vec{v} \oplus \vec{u} \tag{4.1}$$

$$\vec{y}_a : \quad \begin{pmatrix} r & = & \frac{1}{2}\ln\left(\frac{1+|\vec{a}|}{1-|\vec{a}|}\right) \\ \vartheta & = & \vartheta_a \\ \varphi & = & \varphi_a \end{pmatrix} \tag{4.2}$$

$$\vec{y}\prime = \vec{y}_v + \vec{y}_u \qquad \text{(normal vector-addition)} \tag{4.3}$$

$$\vec{v}\prime : \qquad \begin{pmatrix} |\vec{v}\prime| & = & \frac{\exp(2|\vec{y}\prime|)-1}{\exp(2|\vec{y}\prime|)+1} \\ \vartheta\prime & = & \vartheta_{y\prime} \\ \varphi\prime & = & \varphi_{y\prime} \end{pmatrix} \tag{4.4}$$

When a marker crosses the border of a fluid cell, then its current propagation $\vec{r}\prime = \vec{r} + \vec{v} \cdot \mathrm{d}t$ will be finished with the old velocity, i.e. no deflection happens at the border of two cells. This is justified because the timestep $\mathrm{d}t$ is much smaller than the dimensions of the cells $\mathrm{d}x$, $\mathrm{d}y$ and $\mathrm{d}z$, so this will not happen all the time and will not cause too big an error.

If a marker leaves the system, it is deleted. No particle emission at this point is assumed, and the wave is also not reflected.

## 4.3 Freeze-out of the sound wave

In the following we will discuss how to extract spectral enhancements from the position of the wave markers. This is not at all trivial. To explain why a certain method does or does not work, we will refer to the analytical test case of a static medium. Unless explicitly denoted, we claim that the argumentation is valid for non-static medium as well, but would be a lot more complicated to explain.

### 4.3.1 Why trivial addition does not work

A trivial way to evaluate the wave-markers is to assign a certain magnitude of perturbation to each of them and add this to the current cell's momentum and energy density. This may be done with a positive "delta"-function that adds a value at the exact point of the marker, or with a smoother function that adds values at the position of the marker, but also before and after that; presumably, since we want to consider sound-like perturbations, we should add as much energy-momentum as we subtract at another place. The latter might also simulate a kind of interference between different wave-markers.

This way is a good physical choice in order to obtain spatial information about the perturbations. If such a spatial picture of the mach waves is to be made, this is the way to go. This is, in fact, what nature does, and what helps us to make photographs of aeroplanes or bullets (see figure 4.1) showing a clearly visible mach cone.

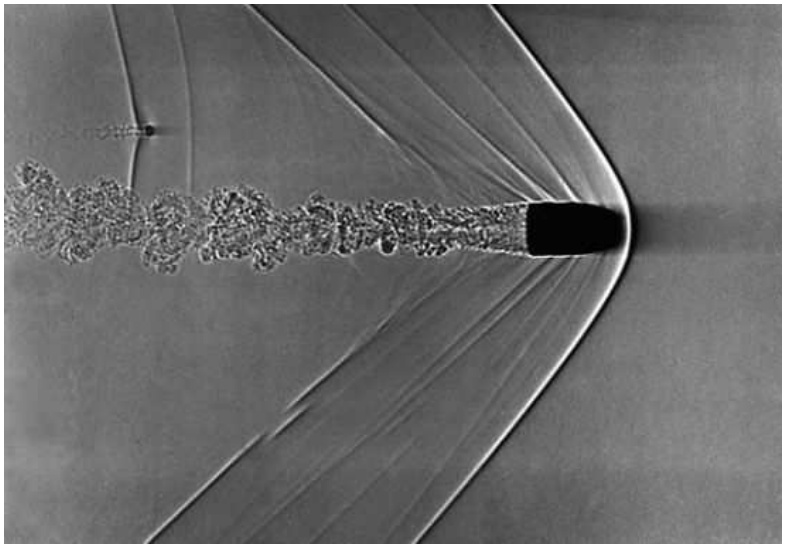

Figure 4.1: A picture of a bullet moving through water. The bullet is moving faster than the speed of sound in the medium, therefore a mach cone develops. From [77].

Unfortunately, a picture of the mach cone is not asked for. We try to achieve a momentum distribution of the system, since this is what will be measured. The momentum distribution of a system altered using the above method will be equal to the unaltered distribution (or enhanced, if energy and momentum have only be added). Using constant time freeze-out (see section 2.4) we integrate over the whole "picture" and pick up the contributions along the mach cone that we saw on the picture. We could see it since their magnitude has been big due to the sheer number of wave markers in close proximity. But we also pick up the contributions opposite to it that do not contribute to the picture. They are not visible because there are only some at relatively big distances. Nevertheless, even if we would not discover their contribution on a spatial picture, their integral remains the same, no matter if they are close to each other or far apart, so they will cancel the contribution of the mach cone.

Not even the interference one might build in will help here, because integration is a linear operation. Taking all perturbations, squaring them and adding them to the system, which would only "count" the amplitudes and

resolve the "integral is constant"-problem, will lose all information about the waves direction. These effects are not unphysical and exactly what would happen with the air perturbed by a supersonic plane. The problem arises with the heavy-ion-way of measuring. When studying a plane we take a picture and look at where the mach cone is. This means we look at the amplitude. If we do not take several pictures, we have, in fact, no idea on where the sound wave will be at a later time step. Another way on how to watch a fast plane is to stand still and listen. We can hear the perturbation. The analogous thing to do in the hydro-evolution is to go to one place and wait for the wave to come — i.e. freeze out at constant place. Due to the assumption that particles will not change their direction after freeze-out spatial information would directly be mapped to momentum information. This method fails for the used freeze-out method (see again section 2.4, page 13).

### 4.3.2 A coalescence-like model

Following the idea that in the wave front many wave markers are close to another and going into the same direction, it might be a good idea to only consider markers that satisfy this condition. It would require two new parameters; the distance in which a different marker is looked for, and a maximal angle by which the directions of the two markers may deviate.

Unfortunately, one finds that in the analytic test-case the distance between two markers emitted into the same direction $\alpha$ at to subsequent timesteps, will be $dr = dt\sqrt{1 + c_S^2 - 2c_S\cos(\alpha)}$, which will be minimal at $\alpha = 0$. Forward markers can therefore not be excluded by this method, although they do not contribute to the mach cone.

This ansatz anyways has not much to do with interference; markers in short distances in the direction of their movement will rather interfere than contribute to collective movement. Markers that are next to each other, though, will contribute. This fact might be taken into account by not using the distance of two markers as criterion. Instead, one can model the distance in a different way:

Usually, one can reinterpret the concept of distance between $\vec{r}$ and $\vec{r}\prime$ as taking a sphere around the point $\vec{r}$ and adjusting the radius so that $\vec{r}\prime$ is on the surface of that shell. The radius $d_{\text{sph}}$ is then the usual — spherical — distance between the points.

The idea that is to be presented here is not to take a sphere and adjust its radius, but to take an ellipsoid with given excentricity and adjust the

remaining parameter (one of the semi axes) so that the second point is on the shell of the ellipsoid.

For these assumptions it is reasonable to have the semi-axes of the ellipsoid aligned along the direction $\hat{v}$ of the considered wave marker; the ellipsoidal should be symmetric in the azimuthal direction with respect to $\hat{v}$. In fact, the semi-axis parallel to $\hat{v}$ is, for the reasons stated above, the shortest.

The (implicit) equation for an ellipsoid satisfying the above constraints having semi-axes $A$ orthogonal and $B$ longitudinal to $\hat{v}$ is

$$\frac{\left(\hat{v}(\vec{r\prime}-\vec{r})\right)^2}{B^2} - \frac{\left(\hat{v}(\vec{r\prime}-\vec{r})\right)^2}{A^2} + \frac{\left(\vec{r\prime}-\vec{r}\right)^2}{A^2} = 1 \quad . \tag{4.5}$$

With given ratio $B = zA$ this becomes $A^2 = (1-z^2)\left(\hat{v}(\vec{r\prime}-\vec{r})\right)^2 + \left(\vec{r\prime}-\vec{r}\right)^2$. $A$ is what we refer to as elliptic distance $d_{\mathrm{ell}}$. Note that it becomes the spherical distance for $B \to A$, i.e. $\lim_{z\to 1} d_{\mathrm{ell}} = d_{\mathrm{sph}}$.

In the same case as above we can now calculate $d_{\mathrm{ell}}$ as a function of $\alpha$. It turns out that we indeed have a maximum for $d_{\mathrm{ell}}$ at forward directions now instead of a minimum, and a minimum at $\cos(\alpha) = \pm B^2\, c_S/(B^2 - A^2)$, which is, though, always smaller than the expected angle $\cos(\alpha) = c_S$. To reach it, one would have to set $A = 0$, which is not reasonable. Using this ansatz would hence always underestimate the angle.

### 4.3.3 What else can be done: The Mantle Method

There *is* a way of looking at a picture of a mach cone and predicting where it will be in the next instant; we consider the movement to be perpendicular to the wave-front. Finding out the directions perpendicular (or parallel) to the front is easy to do by hand, one "sees" where the front goes. It is not so easy to find an algorithm that discovers these directions automatically.

Our approach is to try and reshape the region occupied by wave markers with a set of lines, referred to as *wave-lines*. This surface will be interpreted as the wave front.

The wave lines are equally distributed azimuthally around the jet's direction $\hat{v}$. Their nodes are positions of marker particles. The rough idea is to go in opposite direction of the jet, starting at its position, so that seen from the jet it looks like standing at the pole of the earth and considering the longitudes going away covering the surface of the earth (apart from the earth being a sphere, not a cone).

For the construction of each wave line, a subset of all wave markers is considered. A slice azimuthal to the jet axis is taken into account for every wave line. The center of the azimuth, though, is not necessarily on the trajectory of the jet, but is the geometrical center ("center of mass", though no masses are present) of a given elementary wave, so it changes for markers from different elementary waves. The azimuthal slice is classified by an angle $\phi_{\text{line}}$. It is the angle between the plane spanned by $\hat{v}$ and the wave line on the one side and the plane spanned by $\hat{v}$ and $\hat{a}$ on the other side, where $\hat{a}$ is some arbitrary, fixed direction perpendicular to $\hat{v}$. We shall use the convention

$$\hat{a} \stackrel{\text{def}}{=} \frac{\hat{v} \times \hat{z}}{|\hat{v} \times \hat{z}|} \tag{4.6}$$

$$\hat{b} \stackrel{\text{def}}{=} \hat{v} \times \hat{a} \quad , \tag{4.7}$$

where $\hat{z}$ points in the z-direction[2]. We call the right-handed coordinate system $\hat{v}, \hat{a}, \hat{b}$ the *vab*-system.

Now, we can classify the wave markers by assigning them a similarly defined angle, $\varphi_{\text{marker}}$. In principle, this angle is no different from $\phi_{\text{line}}$, but we allow the intersection line between the two respective planes to change: While the $\hat{v}$–$\hat{a}$ plane remains a constant reference, the second plane is now spanned by $\hat{v}$ and the difference vector of the wave marker $\vec{r}_j$ and the geometrical middle $\vec{r}_{\text{GM}}$ of its elementary wave $\vec{r}_{\text{diff}} = \vec{r}_j - \vec{r}_{\text{GM}}$ (as indicated above). It should be noted that for these considerations it is important to track the sign of the angle.

This problem can be composed into a projection of $\vec{r}_{\text{diff}}$ onto the $\hat{a}/\hat{b}$-plane and the angle between that projection and $\hat{a}$. Considering $\vec{r}_{\text{diff}} = A\hat{a} + B\hat{b} + V\hat{v}$, the projection is $\vec{r}_\perp = A\hat{a} + B\hat{b}$. The angle is then

$$\varphi_{\text{marker}} = \arccos\left(\frac{A}{\sqrt{A^2 + B^2}}\right) \operatorname{sgn}(B) \tag{4.8}$$

where $A = (\vec{r}_j - \vec{r}_{\text{GM}}) \cdot \hat{a}$ and $B = (\vec{r}_j - \vec{r}_{\text{GM}}) \cdot \hat{b}$ are the projections of $\vec{r}_\perp$ towards $\hat{a}$ and $\hat{b}$.

For a given wave line with $\phi_{\text{line}}$ we define a new coordinate system *vfg*($\phi$)

[2]This choice for $\hat{a}$ is practical since we do not consider events with the jet going into the longitudinal direction $\hat{z}$, so we do not have to check whether $\hat{a}$ is non-zero.

which is defined by

$$\hat{f} \stackrel{\text{def}}{=} \cos(\phi)_{\text{line}}\,\hat{a} + \sin(\phi)_{\text{line}}\,\hat{b} \quad \text{and} \tag{4.9}$$

$$\hat{g} \stackrel{\text{def}}{=} \hat{v} \times \hat{f} \quad . \tag{4.10}$$

Furthermore, all wave markers with $\varphi^i_{\text{marker}} \in [\phi_{\text{line}} - \Delta\phi/2; \phi_{\text{line}} + \Delta\phi/2)$ are considered as nodes, where $\Delta\phi = 2\pi/N_{\text{lines}}$ is the angle between two wave lines.

The sheer surface of the area might be very distorted or irregular due to numerical reasons. For instance, due to the finite number of timesteps, the surface will contain large portions of the same elementary waves (in the limit of infinitely many elementary waves each of these only contribute one point, which is a circle in a plane orthogonal to the jet's direction). In order to account for this numerical problem, one has to maximize the angle between the wave line and the jet axis when looking for the next node. This angle, denoted $\alpha$, between a node $\vec{r}_i$ and a candidate $\vec{r}_j$ has to be maximized. It can be written analogous to (4.8):

$$\alpha \stackrel{\text{def}}{=} \arccos\left(\frac{-V}{\sqrt{V^2 + F^2}}\right) \operatorname{sgn}(F) \tag{4.11}$$

where $-V$ and $F$ are the projections of $\vec{r}_i - \vec{r}_j$ onto $-\hat{v}$ and $\hat{f}$, respectively.

Another numerical aspect is the random direction of the wave markers and their finite number. It might be the case that in the area where a given elementary wave should represent the surface there is no wave marker to determine a possible node. Therefore, one has to give the possibility to skip a single elementary wave and go straight onto the second next one without any node taken from the next. Allowing for more than one elementary wave to be ignored may conceal physical effects when collective flow is going into different directions at different points. Figure 4.2 sketches the mentioned cases and shows the surfaces without and with the named improvements.

The search for the next node holds one additional pitfall: since the possible wave markers are not all in one plane, a slight deviation might occur and the wave line might finally drift out of its domain; in the worst case, all lines would end up with the same nodes after some distance. Therefore we have to ascertain the azimuthal position of the wave lines. Hence, the nodes do not correspond to actual positions of wave markers, but to their rotation onto the fixed $\hat{v}/\hat{f}$-plane. Since we can assume that the number of lines is big

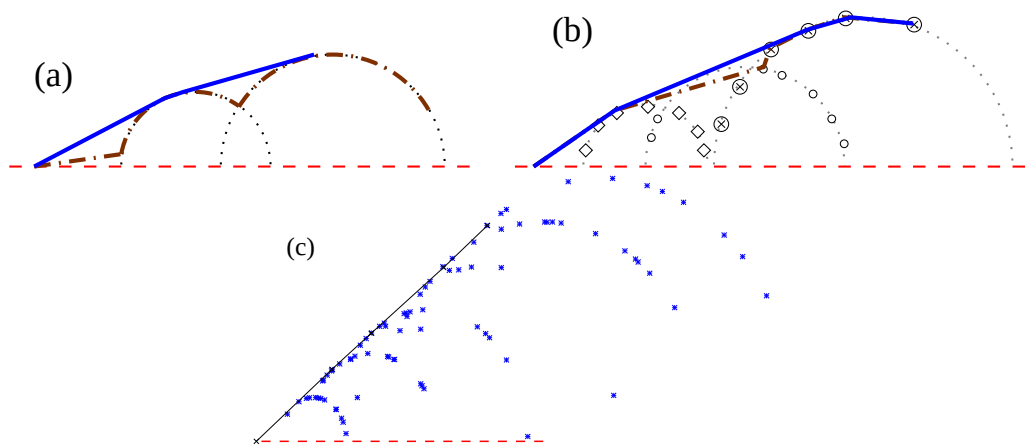


Figure 4.2: A schematic view on how the lines are constructed, assuming that all wave markers are in a common plane. In (a) the basic smoothing is shown (maximizing the angle). In (b) the effect of leaving out single timesteps is shown. Finally, in (c) a dynamically created wave line from data in static medium is shown.
The dashed line shows the jet-trajectory, the dotted arcs the elementary sound waves, the dash-dotted lines the wave lines how they would be without optimization and the solid lines the final wave lines.

enough to provide small angle approximations for $\mathrm{d}\phi$, we do not rotate, but merely project the vector onto that plane. From a candidate $\vec{r}_j$ we therefore get a new node $\vec{r}_{i+1}$ with

$$\vec{r}_{i+1} \stackrel{\text{def}}{=} \vec{r}_j - [\hat{g}(\vec{r}_j - \vec{r}_{\text{GM}})]\,\hat{g} \tag{4.12}$$

When looking for the next node, we have to exclude $\vec{r}_j$. To make the algorithm faster one can exclude all wave markers that lie "behind" the current node (that means, closer to the position of the jet). This can be checked by the relation $(\vec{r}_j - \vec{r}_i)(-\hat{v}) > 0$, from which follows

$$\vec{r}_j\hat{v} < \vec{r}_i\hat{v} \tag{4.13}$$

When all nodes are collected, particle flow is considered to be orthogonal to the wave lines. The lines are taken *as is*. To find the places on which

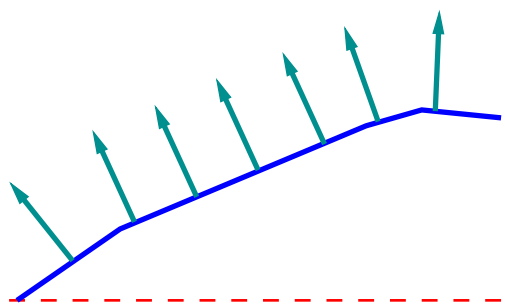

Figure 4.3: Particle flow is assumed to be at fixed distances (the length of the wave line is measured) perpendicular to the current connection between next and previous position. No additional smoothing is done. Also it is not compensated if two or more nodes lie between two "freeze-out-points".

to insert momentum we go along the wave lines, starting from the jet, and insert momentum after fixed distances. Momentum is inserted in the $\hat{v}/\hat{f}$-plane orthogonal to the wave line. No special treatment for momentum insertion at a node is done; orthogonality refers here to the part of the wave line before the respective node (see figure 4.3).

## 4.4 Energy-conservation

As indicated before in the beginning of this chapter (page 23), energy cannot be conserved in this approach. When counting the positions of momentum insertion before defining the amplitude of insertion one can, after measuring the distance $l$ the jet has been going already, set the total amount of energy inserted $\Delta E$ to

$$\Delta E = \left.\frac{\mathrm{d}E}{\mathrm{d}x}\right|_{E\to\infty} l \quad , \tag{4.14}$$

where $\mathrm{d}E/\mathrm{d}x|_{E\to\infty}$ is taken from a different calculation. This will assure that the energy deposited in the mach region is monotonous increasing with time and has reasonable values.

## 4.5 Perfect Background Subtraction

When the system is altered to contain the information of the sound waves, the momentum space distribution (and in principle the whole phase space distribution) can be evaluated to give interesting values. Actually, for two- and three-particle correlations, background from radial, directed and elliptic flow has to be subtracted in order to see a signal. For experiments, background determination and subtraction is a major task.

In the theoretical approach taken, it is possible to do two different things: One could take the original system and try to reproduce the analysis that has to be done in experiments. This would allow for better direct comparison to experimental results, but the data would be specific to a special experiment and background subtraction method. Comparison to data extracted with future, possibly better, methods would not be very easy.

The other way is what we call "perfect background subtraction". The idea is to leave out the background from the beginning. In this method, the system is not, as indicated in section 4.3.3, altered, but the information about where the system would be altered — the clean signal — is evaluated directly. This will result in the cleanest possible signal which would represent the limit of experimental evaluations.

Here, we also have no need for correct estimation of jet energy loss, since we only need to consider that all alterations of the system have the same magnitude.

# Chapter 5

# Results from MACE

There will basically be four different kinds of plots used in this chapter, which are now explained briefly.

First of all, two-particle azimuthal correlations $\mathrm{d}N/\mathrm{d}(\Delta\varphi)$ vs. $\mathrm{d}(\Delta\varphi)$ will be presented, where the near-side jet usually creates a maximum at $\Delta\varphi = 0$. This peak will not be visible in our plots, since in MACE there is no near-side jet. The graphs in those plots show how many particles have been present at an angle $\varphi_i = \varphi_{\mathrm{jet}} + \Delta\varphi$. Since I have no particles in my model, the $\hat{y}$-axis here is in arbitrary units, it counts insertions in the respective direction. Cmp. figures 3.1 and 3.2.

A little more detailed insight to the actual situation might be taken in a three-dimensional two-particle correlation $\mathrm{d}^2N/\mathrm{d}(\Delta\varphi)/\mathrm{d}(\Delta\vartheta)$ vs. $\mathrm{d}(\Delta\varphi)$ and $\mathrm{d}(\Delta\vartheta)$. On the $\hat{y}$-axis, there is a second independent variable, the difference polar angle $\Delta\vartheta = \vartheta_i - \vartheta_{\mathrm{jet}}$, analogous to $\mathrm{d}(\Delta\varphi)$, which is again on the $\hat{x}$-axis. The colours indicate how many particles have been at the respective angles with respect to the jet.

Very similar is the three-dimensionally plotted two-particle correlation $\mathrm{d}^2N/\mathrm{d}(\Delta\varphi)/\mathrm{d}(\Delta\eta)$ vs. $\mathrm{d}(\Delta\varphi)$ and $\mathrm{d}(\Delta\eta)$, where $\mathrm{d}(\Delta\eta)$ is the difference in pseudorapidity between jet and particle.

Both these three-dimensional two-particle correlation only give new insight for an event-by-event analysis. If data are accumulated over many events and then correlated, they become no more meaningful as the (easier to understand and produce) two-dimensional plots.

More insight, even over a sample of many events, can be taken with three-particle correlations $\mathrm{d}N^2/\mathrm{d}(\Delta\varphi_1)\mathrm{d}(\Delta\varphi_2)$ vs. $\mathrm{d}(\Delta\varphi_1)$ and $\mathrm{d}(\Delta\varphi_2)$. Here, the colours ("$\hat{z}$-axis") denote how many particles have been present at an angle

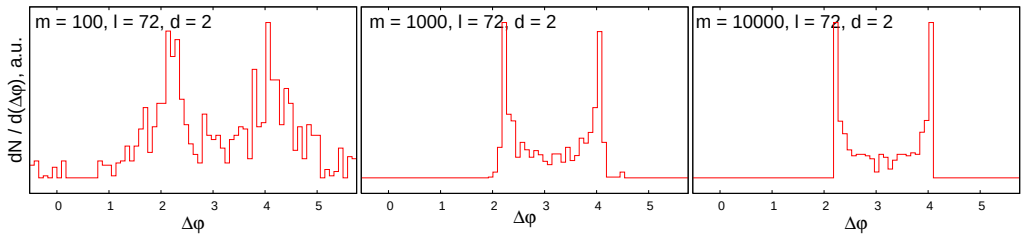


Figure 5.1: The influence of the number of wave markers $m$ on two-particle correlations (in static medium, after 10 time steps). From left to right, the number of wave markers goes up by a factor of 10 between the graphs. While the raising of $m$ from 100 (left) to 1000 (middle) gives a much better signal, the improvement between 1000 and 10 000 does not change the quality a lot.

of $\Delta\varphi_1$ while another particle has been present at $\Delta\varphi_2$. Given that the correlations are done on an event-by-event-basis, a signal here will not be concealed or artificially created by adding the data from many events. Cmp. figures 3.3 and 3.4.

The impact parameter is always given in fractions of the maximum possible impact parameter, which is the sum of the radii of the involved nuclei. E.g., for gold-gold collisions, $b = 10\ \% \equiv 0.1 \cdot (2 \cdot R_{\mathrm{Au}}) \approx 1.36$ fm.

## 5.1 Characterizing the algorithm

The first thing that should be done with a new model or algorithm is to test it with an analytic test case or a known approximation (whichever is applicable), and, in the case of an algorithm, to test it against its behaviour when changing unphysical, numerical parameters.

The analytic test case I am referring to is a static medium, i.e. a system that has a collective flow velocity $\vec{u} \equiv 0$ everywhere and at all timesteps. The algorithm is the one described in chapter 4, especially in sections 4.1, 4.2, 4.3.3 and 4.5.

When taking the approach as described in section 4.5, namely not adding momentum to a hydro system and freezing out afterwards, there are three numerical parameters left in the MACE-model: The number of wave markers created at each timestep $m \equiv n_{\mathrm{marker}}$, the number of wave lines $l \equiv n_{\mathrm{lines}}$ and the number of momentum insertions $d \equiv n_{\mathrm{points}}$ per one $\mathrm{d}t$ length of a wave-line, where $\mathrm{d}t$ is the length of one timestep.

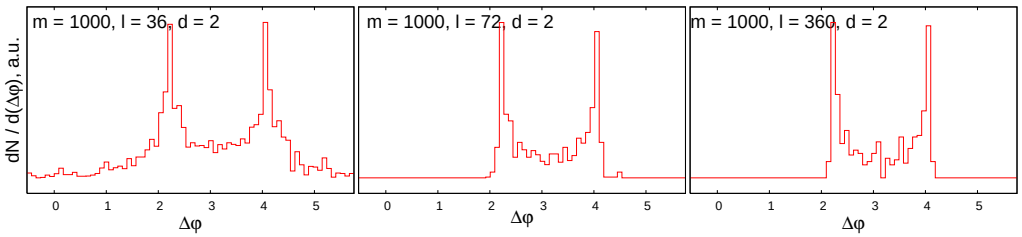


Figure 5.2: The influence of the number of wave lines $l$ on two-particle correlations (in static medium, after 10 time steps). From left to right, the number of wave lines goes up. While the raising of $l$ from 36 (left, corresponds to an angle of $\Delta\phi_{\text{line}} = 10°$) to 72 (middle, $\Delta\phi_{\text{line}} = 5°$) gives a much better signal, the improvement between 72 and 360 ($\Delta\phi_{\text{line}} = 1°$) does not change the quality a lot.

With static medium and no thermal smearing being done, the resulting signal with perfect parameters should be very sharp. With imperfectly shaped surface, the angular distributions will be much wider, since, when the lines are jagged, the normals will be in arbitrary directions. In the two-particle correlations shown in figures 5.1, 5.2 and 5.3, the expectation is not to get two delta-functions. Instead, between the peaks the correlation function should behave similar to an inverse circle, see section 3.1 and equation (3.6). Outside of this region, it should indeed be zero.

Figures 5.1, 5.2 and 5.3 show two-particle correlations $\mathrm{d}N/\mathrm{d}(\Delta\varphi)$ for different values of $m$, $l$ and $d$. The plot in the middle is the same in all figures; it is made with the values that are actually used. In 5.1 and 5.2 it

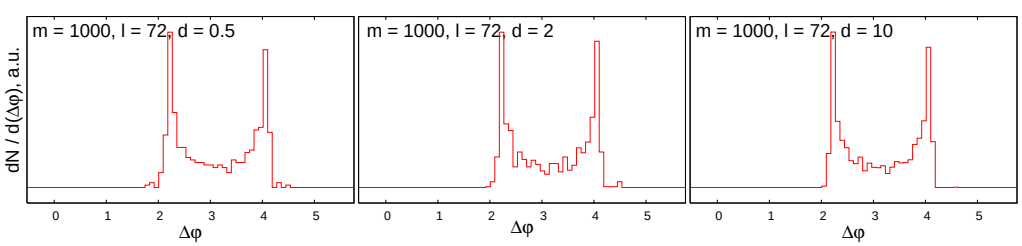


Figure 5.3: The influence of the density of momentum insertions $d$ on two-particle correlations (in static medium, after 10 time steps). From left to right, the density of momentum insertions goes up. Neither step seems to change the plots a lot.

can be seen that the quality improves a lot from the worst chosen resolution to the middle one, but only minor changes appear above that. The signal seems to be rather independent on the density of momentum insertions $d$ (cmp. figure 5.3).

It should be emphasized what the parameters change: A bigger $m$ makes the wave lines smoother, while $l$ and $d$ increase the total number of momentum insertions $N$. Correlation is an $\mathscr{O}(N^2)$-algorithm, so both $l$ and $d$ should be as small as is reasonable.

All in all, it can be concluded that the algorithm shows convergent behaviour with respect to the parameters, so finite values can be taken. In the following subsections, unless differently denoted, all evaluations are made using the values $m = 1\ 000$, $l = 72$ and $d = 2$.

## 5.2 Mach cones at RHIC

In the following section, we discuss the results for correlation functions in gold on gold-collisions at $\sqrt{s_{NN}} = 130$ GeV for different impact parameters. The influence of jet triggers (both direction and origin) is examined in section 5.3 on central LHC-collisions.

### 5.2.1 Central collisions

The central RHIC data, when averaged over 1 000 different jet origins and directions, yield a double-peaked two-particle correlation function and two off-diagonal peaks in the three-particle correlations (see figure 5.4). The maximum of the correlation, however, is shifted from the mach angle of $\alpha \approx 0.96$ "outwards" by about $\delta\alpha \approx 0.2$ radians. The corresponding speed of sound to this angle is $c_S^{2,\ \mathrm{app.}} \approx 0.17$. This value is very close to the expected result for a hadron-resonance gas of $c_S^{2,\ \mathrm{HG}} \approx 0.15$.

### 5.2.2 Mid-central collisions

As the central RHIC data, also the mid-central RHIC data (for impact parameter $b = 25$ %) show two (four) peaks in the two-(three-)particle-correlation function (see figure 5.5). Here, the same deviation from the perfect mach angle is found, which is again much closer to the mach angle of a hadron-resonance gas.

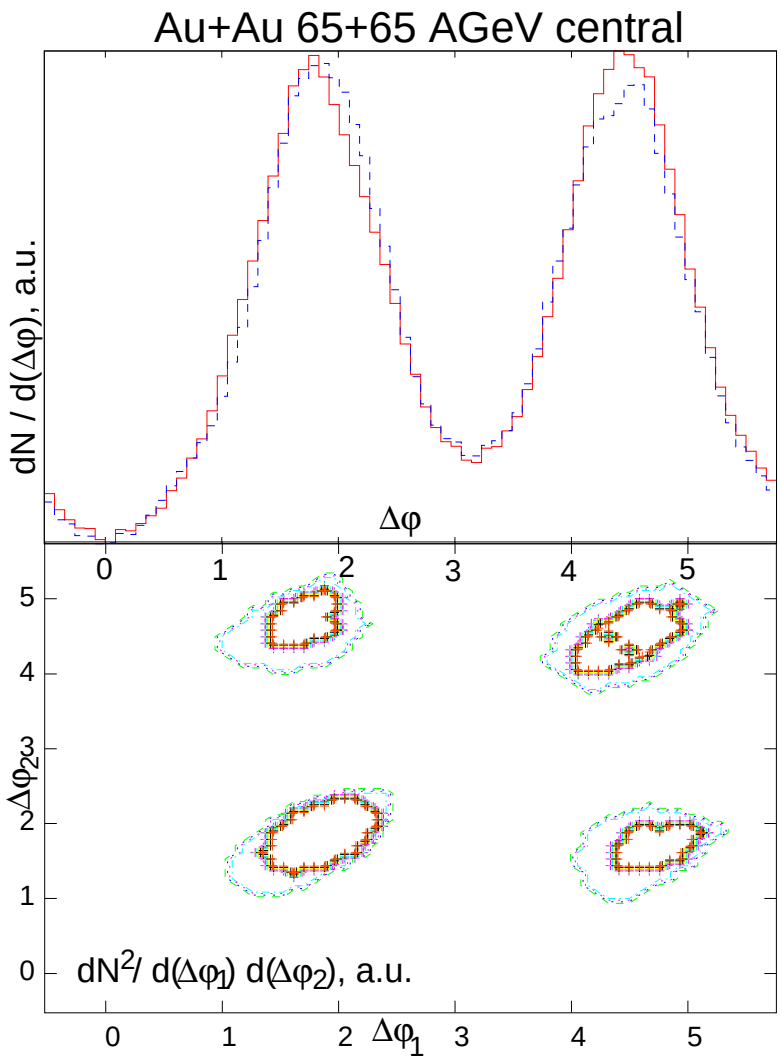


Figure 5.4: Two- and three-particle correlations obtained for central RHIC collisions ($b = 0$ %, red solid line (above) and solid lines (below), and $b = 10$ %, blue dashed line (above) and crosses (below)) at $\sqrt{s_{NN}} = 130$ GeV. The dependent variable is given in arbitrary units.

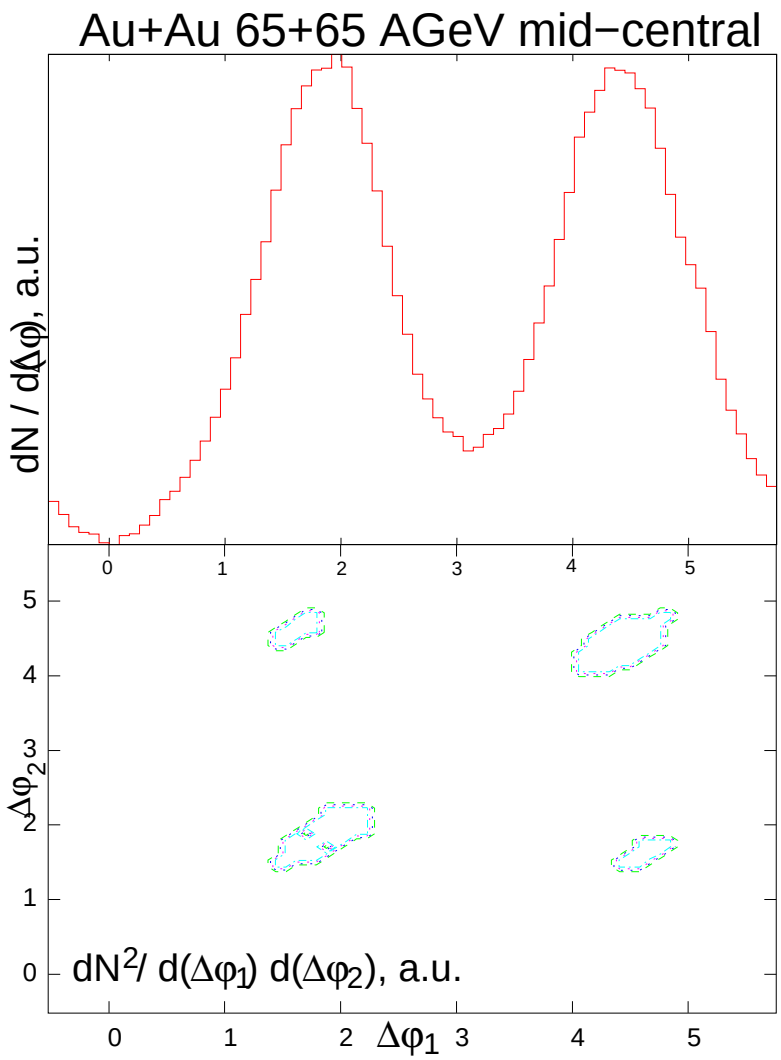


Figure 5.5: Two- and three-particle correlations obtained for central RHIC collisions ($b = 25$ %) at $\sqrt{s_{NN}} = 130$ GeV. The dependent variable is given in arbitrary units.

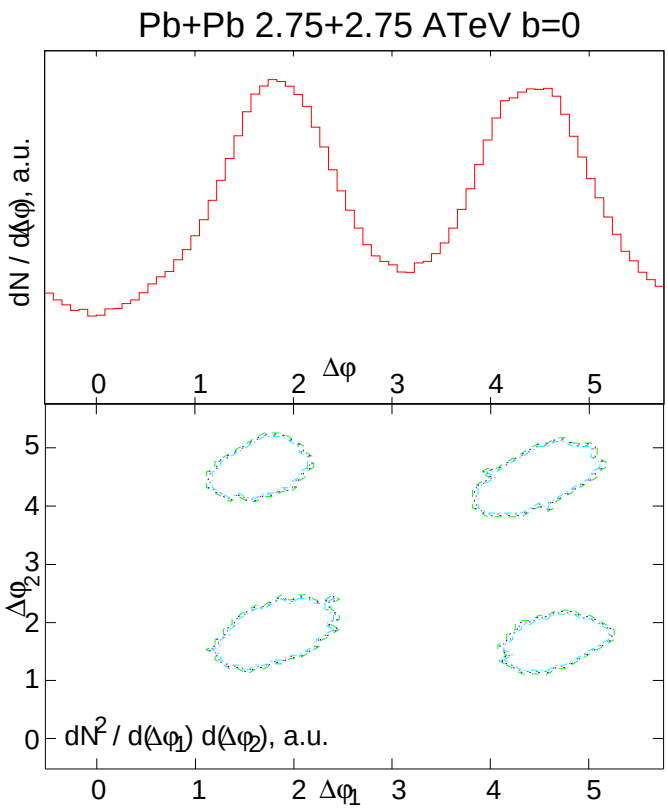


Figure 5.6: Two- (above) and three- (below) particle correlations for central lead-lead-collisions at $\sqrt{s_{NN}} = 5.5$ TeV. These figures show the sum over all correlations from 1 000 events with arbitrary jet orientation and origin.

## 5.3 Mach cones at LHC

In the following section, we discuss the results for correlation functions in lead on lead-collisions at $\sqrt{s_{NN}} = 5.5$ TeV for central collisions.

Correlation functions measured for LHC energies resemble the picture from RHIC. Again, the "minimum jet-bias"-data show a shifted maximum with respect to the mach angle. It is also at $\Delta\phi_{\text{max.}} \approx 1.15$ rad, which corresponds to a speed of sound of $c_S^2 \approx 0.17 \pm 0.07$. The minimum of the correlation function is about 30 % of the maximal value, as has been before. Figure 5.6 (lower part) proves the existence of two maxima in most events (the two off-diagonal peaks). In figure 5.7 two-particle correlations

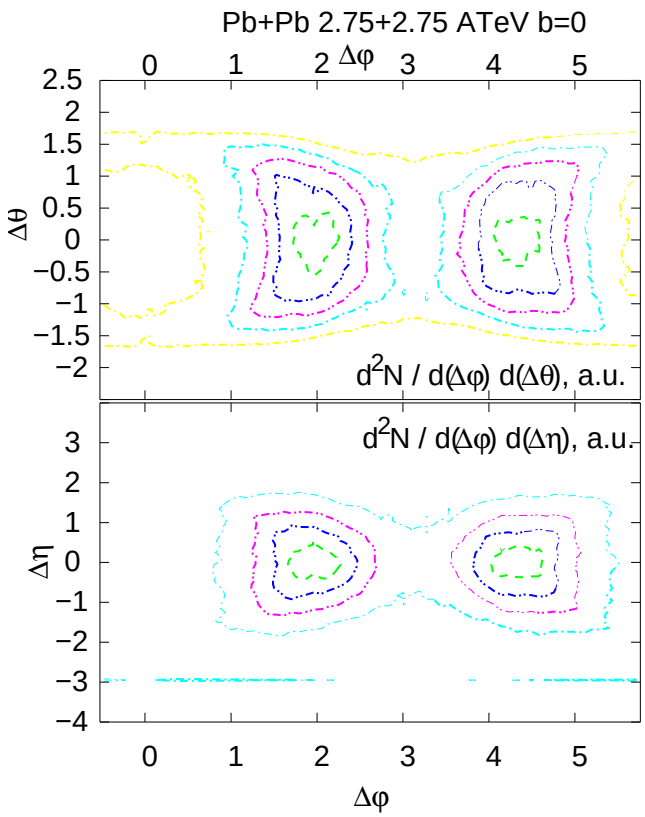


Figure 5.7: Two-particle correlations for central lead-lead-collisions at $\sqrt{s_{NN}} = 5.5$ TeV as function of $\Delta\varphi$ and $\Delta\vartheta$ (a) and $\Delta\eta$ (b). These figures show the same data as figure 5.6. It can be easily seen that these plots do not show the expected ring due to the average over so many events.

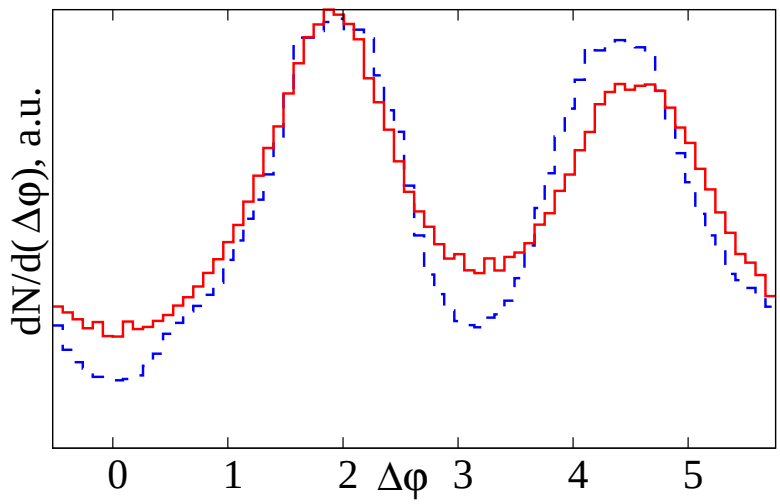


Figure 5.8: Two-particle correlations for central lead-lead-collisions at $\sqrt{s_{NN}} = 5.5$ TeV for two different classes of jets: The red solid line shows the result for $0.4 < \eta_{\rm Jet} < 0.9$, the blue dashed line for $|\eta_{\rm Jet}| < 0.1$.

are plotted for the same set of events, with spatial resolution now also in polar direction. This figure shows why this way of plotting a correlation function is not very helpful; there is no ring structure visible if one considers many events at the same time. All information that can be obtained from these plots is that there is actually never a signal near the near-side-jet, and finite correlations at $\Delta\varphi \approx 0$ come from far away polar positions. The rest is contained in the two-dimensional two-particle correlations already.

In an experiment, several triggers can be applied to the jet. While a trigger on the azimuthal position of the jet does not make sense in the azimuthally symmetric central collisions considered here, it is interesting to take a look at different rapidities of the jet. In figure 5.8 the two-particle correlations for forward jets ($0.4 < \eta_{\rm Jet} < 0.9$) and mid-rapidity jets ($|\eta_{\rm Jet}| < 0.1$) are shown. This is a case where in static medium there *would* be a visible difference. Still, in the moving matter, both correlations look rather similar. Even the mid-rapidity data suggest a different speed of sound than is actually present. The error bars are the same as before.

A much harder task on the experimental side is to find out where a jet

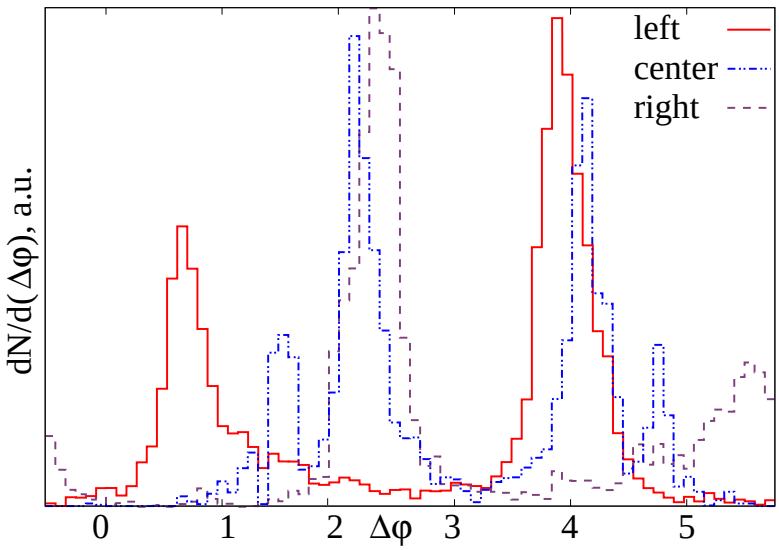


Figure 5.9: Two-particle correlations for mid-rapidity jets in central lead-on-lead-collisions at $\sqrt{s_{NN}} = 5.5$ TeV.

came from. Although this is not directly measurable, the effect of different origins can be studied with MACE. The two-particle-correlation functions for three jets going in mid-rapidity that started next to each other in the center of the collision and left as well as right to that (at 70 % of the way out of the medium) are opposed in figure 5.9. The centrally started jet, finally, shows the behaviour expected in static medium, a symmetric correlation function (symmetric around $\Delta\varphi = \pi$, that is), that peaks at $\Delta\varphi \approx \pi \pm 1$. It is also revealed on this figure how much the starting point of the jet affects the outcome of the mach cone. The left and right jet are, though, pretty mirror-symmetric to each other, having one peak at the mach position and the other at about $\Delta\varphi \approx \pm 0.7$.

Concluding the results, one can say that the double-humped structure is a very robust signal. If there are mach cones in LHC collisions, they should be visible. The maxima, though, are not at the naively expected angle. Only mid-rapidity jets with symmetric correlation functions can give insight on the speed of sound present when the cone was formed. In all other cases, the speed of sound will be underestimated. Due to the steep behaviour of the cosine function at the interesting values around 1 radians, even small

deviations from the perfect mach angle will give completely different results for the speed of sound. Care should therefore be taken to read off a speed of sound from a measured correlation function. There be dragons.

# Chapter 6

# Summary and Outlook

The properties of hot and dense nuclear matter have been subject to a lot of research projects in the last decades. To study this kind of matter, atomic nuclei (so-called *heavy ions*) are collided at very high center of mass energies. From the observable particle spectra researchers try to get information about the different properties of matter.

After the publication of some experimental results of the currently most powerful heavy ion-accelerator, RHIC, it became probable that hydrodynamical descriptions of nuclear matter in such collisions work pretty well.

In Hydrodynamics, the spread of sound waves is intimately connected to the *Equation of State* (EoS). To get information about this it is good to find a signal for (or *from*) sound waves.

A high energetic parton travelling through the medium (a *jet*) might loose its energy by bouncing off other partons. Its energy will then propagate through the medium as sound waves. With an ultra-relativistic jet, i.e. one moving practically with the speed of light, those sound waves would — since the speed of sound is smaller than the speed of light — interfere to form a cone, the so-called *mach cone*, as is the case with an airplane with supersonic velocities.

In the presented thesis the model MACE (MAch Cones Evolution) is developed, which simulates the propagation of sound waves through a medium that itself moves with relativistic speeds in the order of magnitude of the speed of sound.

In Chapter 4 it is shown how this model can be used to simulate the sound waves of a moving source and automatically find collective effects as a mach cone ("supersonic boom") and analyse them. Here, the input needed

is the velocity-distribution of a medium as a function of space and time, in order to propagate the waves with a constant speed with respect to the local rest frame of the medium.

The elementary spherical waves are modelled by logical points. Their entirety represents the sound wave. To recognize the mach cone automatically, the space region in which these points are, is mantled, i.e. the surface is determined. That means that interference-effects are not modelled, but a geometrical procedure is used. The surface is converted into a signal directly, it is abdicated to first create an altered speed profile, as it is accessible to the experiments, to re-obtain the signal from that.

From normals to this surface a spectrum is calculated, which is measured as increased particle emission in the experiments.

MACE is tested for its behaviour when changing numerical parameters in section 5.1. In sections 5.2 and 5.3 MACE is applied to the speed profiles from gold-gold-collisions at $\sqrt{s_{NN}} = 130$ GeV (RHIC) and lead-lead-collisions at $\sqrt{s_{NN}} = 5.5$ TeV (LHC) and the results are presented.

It turns out that, when averaging over many jets, no significant differences between the correlations from different starting points can be seen. Indeed, the added-up correlation functions are indistinguishable from those expected from static medium. Even when considering different special cases on the direction of the jet, the picture does not change. Only when triggering on the origin of the jet, which is experimentally the hardest of all tasks, one can see a pronounced change in the shape of the correlations. Still, for centrally started jets, there is no qualitative difference between LHC-data and static medium.

In all averaged cases considered, the apparent, measured speed of sound is smaller than what has been input to the calculation and what has been used to propagate sound. This effect is strong enough to simulate a hadron gas with $c_S^2 = 0.15$ in favour of the (actually present!) quark-gluon-plasma with $c_S^2 = 1/3$. As stated above, only mid-rapidity jets starting from the middle of the medium (recognizable by rather symmetric correlation functions) can reveal the true speed of sound. It is emphasized that an attempt to read of the speed of sound from an (in terms of the trigger) unqualified correlation function is doomed to fail.

Since the underlying hydrodynamical algorithm (the PIC-Code, see section 2.4) currently only uses an EoS with massless Quark-Gluon-Plasma, it could not be studied how the data change with variable speed of sound. The

porting of MACE to hydro-codes that do use a more complicated EoS and the changing of the speed of sound depending on the properties of the underlying medium will be a future project that may give interesting results.

The next point that may be done with MACE is comparing the results from this approach to the data obtained by inserting a jet during the creation of the hydro-evolution. Here, differences between those models could be studied in detail.

# Appendix A

# Bibliography


[1] Press Release "New State of Matter created at CERN", Febuary 10, 2000

[2] Y. Aoki, Z. Fodor, S. D. Katz and K. K. Szabo, Phys. Lett. B **643** (2006) 46 [arXiv:hep-lat/0609068].

[3] Wikipedia, "Image:QCD phase diagram.png" — Wikipedia, The Free Encyclopedia, April 16, 2006. Image is released into the public domain.

[4] Press Release "RHIC Scientists Serve Up 'Perfect' Liquid", April 18, 2005

[5] F. Becattini and G. Passaleva, Eur. Phys. J. C **23** (2002) 551 [arXiv:hep-ph/0110312].

[6] P. Braun-Munzinger, J. Stachel, J. P. Wessels and N. Xu, Phys. Lett. B **344**, 43 (1995) [arXiv:nucl-th/9410026].

[7] P. Braun-Munzinger, J. Stachel, J. P. Wessels and N. Xu, Phys. Lett. B **365**, 1 (1996) [arXiv:nucl-th/9508020].

[8] J. Cleymans and K. Redlich, Phys. Rev. C **60**, 054908 (1999) [arXiv:nucl-th/9903063].

[9] A. Kisiel, T. Taluc, W. Broniowski and W. Florkowski, Comput. Phys. Commun. **174**, 669 (2006) [arXiv:nucl-th/0504047].

[10] G. Torrieri, S. Steinke, W. Broniowski, W. Florkowski, J. Letessier and J. Rafelski, Comput. Phys. Commun. **167**, 229 (2005) [arXiv:nucl-th/0404083].

[11] S. A. Bass *et al.*, Prog. Part. Nucl. Phys. **41** (1998) 225 [arXiv:nucl-th/9803035].

[12] M. Bleicher *et al.*, J. Phys. G **25** (1999) 1859 [arXiv:hep-ph/9909407].

[13] E. L. Bratkovskaya *et al.*, Phys. Rev. C **69** (2004) 054907 [arXiv:nucl-th/0402026].

[14] G. Boyd, J. Engels, F. Karsch, E. Laermann, C. Legeland, M. Lutgemeier and B. Petersson, Nucl. Phys. B **469** (1996) 419 [arXiv:hep-lat/9602007].

[15] F. Karsch, E. Laermann and A. Peikert, Nucl. Phys. B **605** (2001) 579 [arXiv:hep-lat/0012023].

[16] C. R. Allton *et al.*, Phys. Rev. D **66** (2002) 074507 [arXiv:hep-lat/0204010].

[17] Z. Fodor and S. D. Katz, JHEP **0203** (2002) 014 [arXiv:hep-lat/0106002].

[18] Z. Fodor and S. D. Katz, Phys. Lett. B **534** (2002) 87 [arXiv:hep-lat/0104001].

[19] J. Hofmann, H. Stöcker, W. Scheid and W. Greiner, *Report of the Workshop on BeV/nucleon Collisions of Heavy Ions: How and Why, Bear Mountain, New York, 29 Nov - 1 Dec 1974*

[20] J. Hofmann, H. Stöcker, U. W. Heinz, W. Scheid and W. Greiner, Phys. Rev. Lett. **36** (1976) 88.

[21] D. H. Rischke, [arXiv:nucl-th/9809044].

[22] Laszlo Csernai, *Relativistic Heavy Ion Physics*, TUGboat Volume 9, Issue 1 (1988)

[23] A. A. Amsden and F. H. Harlow J. Comp. Phys **3** 1 (1968) 94-110

[24] A. A. Amsden, A. S. Goldhaber, F. H. Harlow and J. R. Nix, Phys. Rev. C **17** (1978) 2080.

[25] R. B. Clare *et al.* Phys. Rept. **141** (1986) 177,

[26] D. Strottman, Lecture Notes in Mathematics 1385: (1989) 278-289 and

[27] N. S. Amelin, E. F. Staubo, L. P. Csernai, V. D. Toneev, K. K. Gudima and D. Strottman, Phys. Lett. B **261** (1991) 352.

[28] V. K. Magas, L. P. Csernai and D. D. Strottman, Phys. Rev. C **64** (2001) 014901, [arXiv:hep-ph/0010307].

[29] M. Zétényi, private communication

[30] J. Adams *et al.* [STAR Collaboration], Phys. Rev. Lett. **91** (2003) 072304 [arXiv:nucl-ex/0306024].

[31] R. Baier, Y. L. Dokshitzer, A. H. Mueller, S. Peigne and D. Schiff, Nucl. Phys. B **484** (1997) 265 [arXiv:hep-ph/9608322].

[32] R. Baier, Y. L. Dokshitzer, A. H. Mueller, S. Peigne and D. Schiff, Nucl. Phys. B **483** (1997) 291 [arXiv:hep-ph/9607355].

[33] B. G. Zakharov, JETP Lett. **63** (1996) 952 [arXiv:hep-ph/9607440].

[34] M. Gyulassy, P. Levai and I. Vitev, Phys. Rev. Lett. **85** (2000) 5535 [arXiv:nucl-th/0005032].

[35] M. Gyulassy, P. Levai and I. Vitev, Nucl. Phys. B **594** (2001) 371 [arXiv:nucl-th/0006010].

[36] M. G. Mustafa and M. H. Thoma, Acta Phys. Hung. A **22** (2005) 93 [arXiv:hep-ph/0311168].

[37] J. D. Bjorken, FERMILAB-PUB-82-059-THY

[38] M. H. Thoma and M. Gyulassy, Nucl. Phys. B **351** (1991) 491.

[39] E. Braaten and M. H. Thoma, Phys. Rev. D **44** (1991) 1298.

[40] E. Braaten and M. H. Thoma, Phys. Rev. D **44** (1991) 2625.

[41] S. Wicks, W. Horowitz, M. Djordjevic and M. Gyulassy, [arXiv:nucl-th/0512076].

[42] A. Peshier, Phys. Rev. Lett. **97** (2006) 212301 [arXiv:hep-ph/0605294].

[43] A. Peshier, Phys. Rev. C **75** (2007) 034906 [arXiv:hep-ph/0607299].

[44] A. Peshier, Eur. Phys. J. C **49** (2007) 9 [arXiv:hep-ph/0607275].

[45] A. Peshier, [arXiv:hep-ph/0601119].

[46] J. Adams *et al.* [STAR Collaboration], Phys. Rev. Lett. **95** (2005) 152301 [arXiv:nucl-ex/0501016].

[47] F. Wang [STAR Collaboration], Nucl. Phys. A **774**, 129 (2006) [arXiv:nucl-ex/0510068].

[48] H. Stöcker, Nucl. Phys. A **750** (2005) 121 [arXiv:nucl-th/0406018].

[49] I. Vitev, Phys. Lett. B **630** (2005) 78 [arXiv:hep-ph/0501255].

[50] A. D. Polosa and C. A. Salgado, Phys. Rev. C **75** (2007) 041901 [arXiv:hep-ph/0607295].

[51] I. M. Dremin, Nucl. Phys. A **767** (2006) 233 [arXiv:hep-ph/0507167].

[52] A. Majumder, V. Koch and X. N. Wang, Nucl. Phys. A **774**, 561 (2006).

[53] H. Stöcker, J. Hofmann, J. A. Maruhn and W. Greiner, *In *Erice 1979, Proceedings, Heavy Ion Interactions At High Energies*, 133–195*

[54] H. Stöcker and W. Greiner, Phys. Rept. **137** (1986) 277.

[55] D. H. Rischke, H. Stöcker and W. Greiner, Phys. Rev. D **42** (1990) 2283.

[56] G. F. Chapline and A. Granik, Nucl. Phys. A **459** (1986) 681.

[57] A. E. Glassgold, W. Heckrotte and K. M. Watson, Ann. Phys. **6** (1959) 1.

[58] V. A. Khodel, N. N. Kurilkin and I. N. Mishustin, Phys. Lett. B **90** (1980) 37.

[59] J. Casalderrey-Solana, E. V. Shuryak and D. Teaney, J. Phys. Conf. Ser. **27** (2005) 22 [Nucl. Phys. A **774** (2006) 577] [arXiv:hep-ph/0411315].

[60] J. Casalderrey-Solana, [arXiv:hep-ph/0701257].

[61] F. Antinori and E. V. Shuryak, J. Phys. G **31** (2005) L19 [arXiv:nucl-th/0507046].

[62] C. Adler *et al.* [STAR Collaboration], Phys. Rev. Lett. **90** (2003) 082302 [arXiv:nucl-ex/0210033].

[63] L. Molnar, [arXiv:nucl-ex/0701061].

[64] S. S. Adler *et al.* [PHENIX Collaboration], Phys. Rev. D **74** (2006) 072002 [arXiv:hep-ex/0605039].

[65] F. Wang [STAR Collaboration], J. Phys. G **30** (2004) S1299 [arXiv:nucl-ex/0404010].

[66] J. G. Ulery and F. Wang, [arXiv:nucl-ex/0609017].

[67] F. Wang, Nucl. Phys. A **783** (2007) 157 [arXiv:nucl-ex/0610011].

[68] F. Wang, AIP Conf. Proc. **892** (2007) 417 [arXiv:nucl-ex/0610027].

[69] B. Jacak [PHENIX Collaboration], J. Phys. Conf. Ser. **50** (2006) 22 [arXiv:nucl-ex/0508036].

[70] N. N. Ajitanand [PHENIX Collaboration], Acta Phys. Hung. A **27** (2006) 197 [arXiv:nucl-ex/0511029].

[71] J. G. Ulery [STAR Collaboration], [arXiv:0704.0224 [nucl-ex]].

[72] L. M. Satarov, H. Stöcker and I. N. Mishustin, Phys. Lett. B **627** (2005) 64 [arXiv:hep-ph/0505245].

[73] A. K. Chaudhuri, Phys. Rev. C **75** (2007) 057902 [arXiv:nucl-th/0610121].

[74] ALICE Time Projection Chamber, Technical Design Report, Cern/LHCC 2000-001.

[75] H. Stöcker, B. Betz and P. Rau, [arXiv:nucl-th/0703054].

[76] T. Renk and J. Ruppert, [arXiv:hep-ph/0702102].

[77] John Gwynn and sons, "The Water-Rocket Explorer", April 15, 2003, http://waterocket.explorer.free.fr/images/bullet1.jpg.

# Appendix B

# Acknowledgements

My studies and this work have been graciously supported by the German National Academic Foundation and the International Office of Frankfurt University. I want to thank Linus for the kernel, Ian for the distribution, Ben, Brian and Michael for minimizing the file recoveries needed (thanks for those to Xela!), Larry for this incredibly flexible language, Bjarne for the stiff, fast language, Jon S. for the best closed source I have ever worked with, Bram for the editor and Donald and Leslie for the typesetting system.

Thank you Jörg, Werner, Susanne, Anna-Lena, Frank, Tobias, Nathalie, and Tim for the homely sounds, and thank you Pterry for the distraction.

I wish to thank everyone who supported me in the past years. First of all, thanks to my supervisors. László Pál Csernai has given me infrastructure and support during the last year. He taught me a lot and I am thankful each little bit of it. I also thank Horst Stöcker, my official supervisor, for supporting me and believing in me all the time since we first met. His faith in me has always been a big reassurance in times of doubt.

Of the people I have worked with I first want to thank Marcus Bleicher who taught me a vast amount of things about physics, programming, politics and a lot more, and all that without me being his student. Thank you so much.

Thank you L. M. Satarov for fruitful discussions that got the last touch to the thesis.

Also, I would like to thank my colleagues Yun Cheng, Miklós Zétényi and Péter Ván for fruitful physical discussions and Szabolcs Horvat and Boris Wagner for their friendship. Thanks to Aasne Vikøy for teaching me *det*

*norske språket* — it has really been a wonderful course. Further thanks to Hilde, Maren, Øystein, Øyvind (all of you), Hermod, Alex, Therese, Per, Anja and Dieter.

Thank you Gabriela Meyer, clerk to Mr. Stöcker, for doing infinitely many little things that actually made it possible for me to be abroad for one year.

I want to express my gratitude to all of my friends back home in Germany for keeping up friendship and contact over a distance of 1 200 kilometers and one year, namely Sophie Kirschner, Janet Schmidt, Rainer Stiele, Heike Berleth, Carolin Böse, Felix Sturm, Verena Schwenk, Luisa Ickes, Stefan Heckel, Angela Groth, Berit Körbitzer and Gudrun and Gebhard Kabelitz. Thank you Christian Stuck and my uncle Klaus Voigtmann for saving me from the downs of evil Lord Bill and teaching me the (regrettably) Secret Ways Of The Penguin. Especially the shared evenings on the riverside of the Main with Stefan Salm have been a good incentive to finish quickly and come back, and I want further to thank my best friend Johannes Schwenk for his support at the right times.

Thanks to the whole of the students council (Fachschaft Physik) and the guitar orchestra of the music school for youngsters (Jugendmusikschule) Frankfurt for standing me and my moods for so long time and giving me so many hours of pleasure throughout the years.

The deepest gratitudes are expressed last: my parents Marieluise and Peter have supported me all my life and taught me how to live. My Ultra Krasse Sister UKS Melanie has shown me a lot beautiful sides of life and shares many nice experiences with me.

Finally, there is only one more person to mention. My girlfriend Hannah Petersen, who has been and still is dear friend, support, partner, ray of hope, advice, encouragement, reason to live, reason to hurry, reason to be good, dream, corrector and everything else I needed, and most of the time all this at once, to me, has been the best help I could imagine. Without her, I would not have finished this thesis.

Oh, by the way — thank you to *who-ever* invented Äbbelwoi.

# Appendix C

# Legal stuff

## C.1 Deutsche Zusammenfassung der Diplomarbeit — German Abstract to the thesis

Die Eigenschaften von heißer, dichter Kernmaterie sind Gegenstand vieler Forschungsvorhaben der letzten Jahrzehnte. Um solche Materie zu untersuchen, werden Atomkerne (sog. *Schwerionen*) bei extrem hohen Schwerpunktsenergien zur Kollision gebracht. Aus den dabei messbaren Teilchenspektren versuchen die Forscher, Aufschlüsse über verschiedenste Eigenschaften der Materie zu erlangen.

Nach Veröffentlichung einiger Messergebnisse des momentan leistungsfähigsten Beschleunigers für schwere Atomkerne, RHIC, scheint es wahrscheinlich, dass hydrodynamische Beschreibungen für Kernmaterie in solchen Kollisionen recht gut sind.

In der Hydrodynamik ist die Ausbreitung von Schall eng mit der sog. *Zustandsgleichung* der Materie verbunden. Um Aufschluss über diese zu erhalten, ist es daher gut, ein Signal für bzw. von Schallwellen zu finden.

Ein sich durch das Medium bewegendes hochenergetisches Parton (ein *Jet*) kann eventuell durch Stöße mit anderen Partonen Energie verlieren, die dann in Form von Schallwellen durch das Medium propagiert wird. Bei einem ultrarelativistischen Jet, also einem, der sich praktisch mit Lichtgeschwindigkeit bewegt, würden sich — da die Schallgeschwindigkeit kleiner als die Lichtgeschwindigkeit ist — solche Schallwellen zu Kegeln (sog. *Mach-*

*kegel*) überlagern, wie bei Flugzeugen mit Geschwindigkeiten jenseits der Schallmauer.

In der vorliegenden Arbeit wird das Modell MACE (MAch Cones Evolution — Mach-Kegel-Entwicklung) entwickelt, das die Propagation von Schallwellen durch ein Medium simuliert, das sich selbst mit relativistischen Geschwindigkeiten in der Größenordnung der Schallgeschwindigkeit bewegt.

In Kapitel 4 wird gezeigt, wie dieses Modell benutzt werden kann, um die Schallwellen einer sich bewegenden Quelle zu simulieren und kollektive Effekte wie einen Machkegel ("Überschallkegel") automatisch zu finden und zu analysieren. Hierbei wird als Input die Geschwindigkeitsverteilung eines Mediums als Funktion von Ort und Zeit benutzt, um die Wellen mit konstanter Geschwindigkeit im Ruhesystem des Mediums zu propagieren.

Die elementaren Kugelwellen werden dabei durch logische Punkte modelliert, deren Gesamtheit die Schallwelle darstellen. Um den Machkegel automatisch zu erkennen, wird die Raumregion, in der sich diese Punkte aufhalten, ummantelt, d.h. die Oberfläche wird bestimmt. Das bedeutet, dass nicht Interferenz-Effekte modelliert werden, sondern geometrische Überlegungen benutzt werden. Die Oberfläche wird direkt in ein Spektrum umgewandelt, es wird darauf verzichtet, zunächst ein verändertes Geschwindigkeitsprofil zu erstellen, wie es den Experimenten direkt zugänglich ist, um dann das Signal daraus zu ermitteln.

Aus Normalen auf dieser Oberfläche wird dann ein Spektrum ermittelt, das im Experiment als erhöhte Teilchen-Emission gemessen wird.

MACE wird in Kapitel 5 zunächst auf sein Verhalten gegenüber der Veränderung von numerischen Parameter getestet (Abschnitt 5.1). In den Abschnitten 5.2 und 5.3 wird MACE dann auf die Geschwindigkeitsprofile von Gold-Gold-Kollisionen bei $\sqrt{s_{NN}} = 130$ GeV (RHIC) und Blei-Blei-Kollisionen bei $\sqrt{s_{NN}} = 5.5$ TeV (LHC) angewandt und Ergebnisse werden vorgestellt.

Es zeigt sich, dass, wenn über genug Jets gemittelt wird, keine signifikanten Unterschiede zwischen den Korrelationen von verschiedenen Startbedingungen sichtbar sind. In der Tat sind die (aufaddierten) Korrelationsfunktionen nicht zu unterscheiden von denen, die bei statischem Medium erwartet werden. Sogar, wenn man verschiedene Spezialfälle für die Richtung des Jets betrachtet, ändert sich das Bild nicht. Nur bei triggern auf den Ursprung des Jets, was eine sehr schwierige experimentelle Aufgabe ist, kann man eine ausgeprägte Veränderung in der Form der Korrelationen sehen. Doch wieder ergibt sich für zentral gestartete Jets keine qualitative Veränderung zwischen

LHC-Daten und statischem Medium.

In allen betrachteten, gemittelten Fällen verschieben sich die Korrelationsfunktionen so, dass man naiv eine Schallgeschwindigkeit messen würde, die um etwa das eineinhalbfache kleiner ist als die tatsächlich benutzte Schallgeschwindigkeit. Dadurch kann die Existens einer anderen Form von Materie (Hadronengas statt Quark-Gluonen-Plasma) vorgetäuscht werden. Wie oben angedeutet, können nur Jets in Mittrapidität, die in der Mitte des Mediums starten (diese Jets sind erkennbar an einer symmetrischen Korrelationsfunktion), die wahre Schallgeschwindigkeit aufzeigen. Es wird unterstrichen, dass jeglicher Versuch, eine Schallgeschwindigkeit an einer Korrelationsfunktion abzulesen, zum Scheitern verurteilt ist, wenn man nicht genau weiß, auf was getriggert wurde oder der Trigger nicht auf das Problem passte.

## C.2 Erklärung zur Diplomarbeit

Ich versichere hiermit, dass ich die vorliegende Arbeit selbständig verfasst, keine anderen als die angegebenen Hilfsmittel verwendet und sämtliche Stellen, die benutzten Werken im Wortlaut oder dem Sinne nach entnommen sind, mit Quellen- bzw. Herkunftsangaben kenntlich gemacht habe.

Frankfurt am Main, den 11. Juni 2007

Bjørn Bäuchle